Institut für Theoretische Physik

Universität Würzburg

Elektronen mit starker Korrelation:

von “schweren” Fermionen zu Quantendots

M.Kiselev

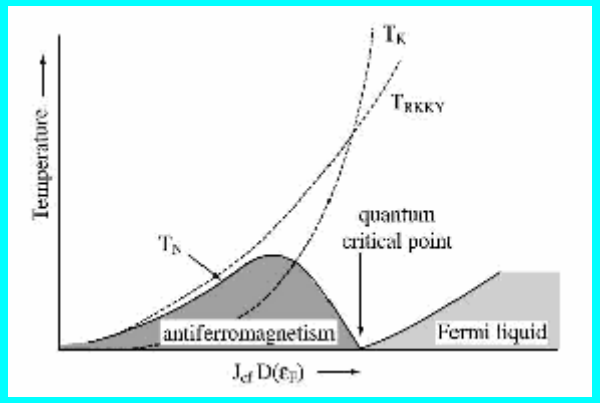

Überblick

- Fermionen: von Teilchen zu Quasiteilchen
- Fermionen: von leichten zu schweren
- Kondo-Effekt: lokale Spin-Korrelationen
- RKKY: nicht-lokale Spin-Korrelationen
- Spin-Flüssigkeit: Resonating Valence Bonds
- Kondo-Effekt und “quantum mirages”
- Kondo-Effekt in Quantendots

Fermionen und Bosonen

$$\Psi(\xi_1,\xi_2) = e^{i\alpha}\Psi(\xi_2,\xi_1)$$

$\alpha = 0$

Bosonen

$\alpha = \pi$

Fermionen

$$\Psi = \frac{1}{\sqrt{N! n_{p_1}! \ldots}} \sum P \psi_{p_1}(\xi_1)\psi_{p_2}(\xi_2)\ldots\psi_{p_N}(\xi_N)$$

$$\Psi = \frac{1}{\sqrt{N!}} \begin{vmatrix} \psi_{p_1}(\xi_1) & \psi_{p_1}(\xi_2) & \ldots & \psi_{p_1}(\xi_N) \\ \psi_{p_2}(\xi_1) & \psi_{p_2}(\xi_2) & \ldots & \psi_{p_2}(\xi_N) \\ \ldots & \ldots & \ldots & \ldots \\ \psi_{p_N}(\xi_1) & \psi_{p_N}(\xi_2) & \ldots & \psi_{p_N}(\xi_N) \end{vmatrix}$$

Das ideale Fermi - Gas

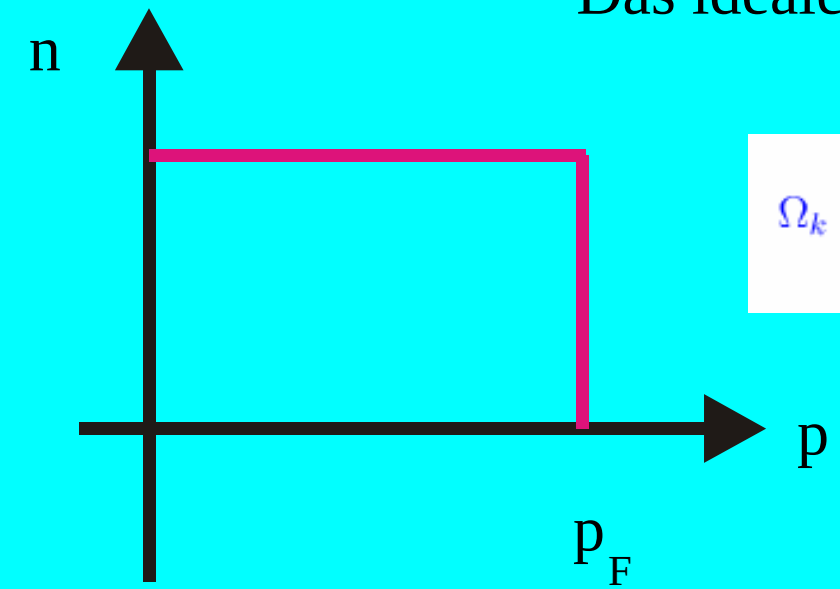

$$\Omega_k = -T \ln \left(\sum_k \left(e^{\frac{\mu - \epsilon_k}{T}} \right)^{n_k} \right) = -T \ln \left(1 + e^{\frac{\mu - \epsilon_k}{T}} \right)$$

$$n_k = 0, 1$$

$$n(\epsilon_k) = \frac{1}{e^{\frac{\epsilon_k - \mu}{T}} + 1}$$

$$N = \int 2 \frac{4\pi p^2 dp V}{(2\pi\hbar)^3} = \frac{V p_F^3}{(3\pi^2 \hbar^3)}$$

Fermi-Flüssigkeits-Theorie

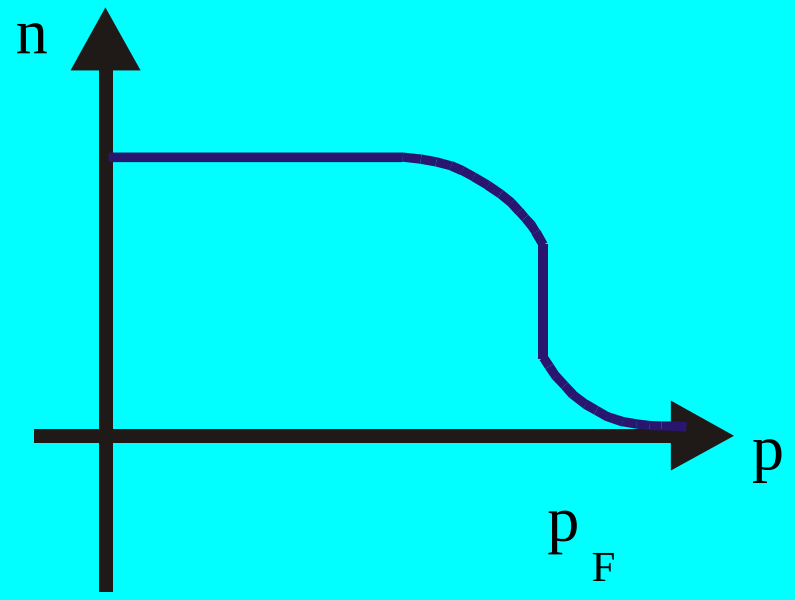

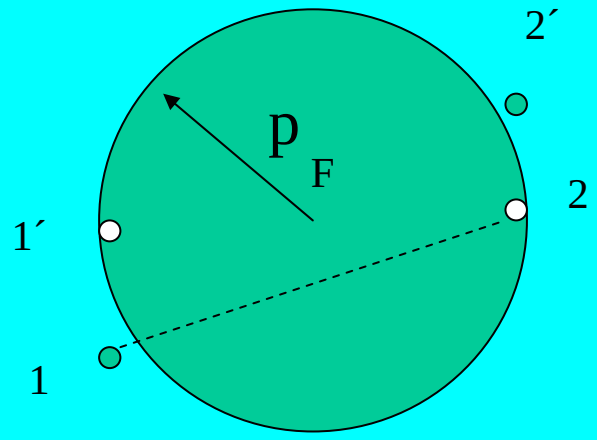

Luttinger Theorem

$$\frac{N_e}{V} = 2q\frac{N}{V} + 2\frac{V_F}{(2\pi\hbar)^3}$$

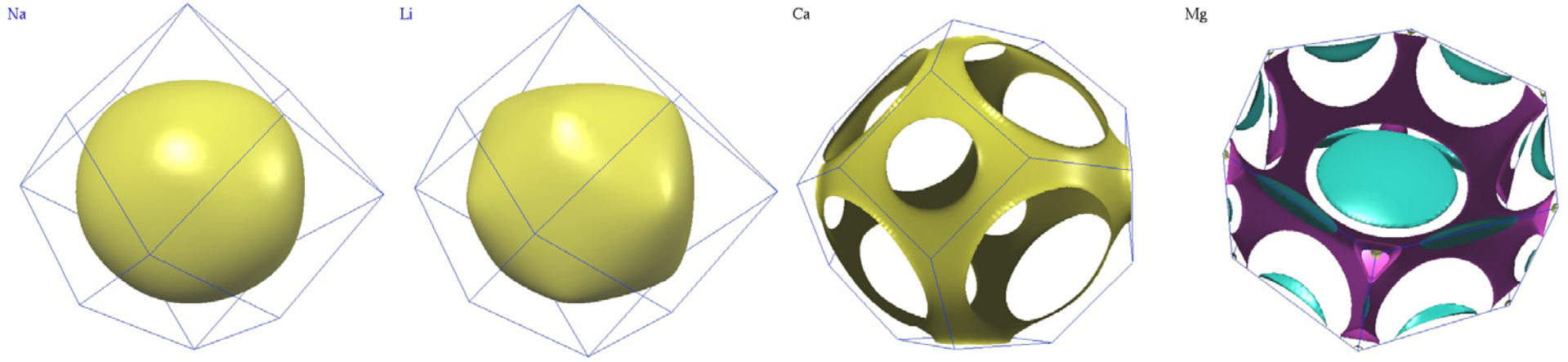
Na
Li
Ca
Mg

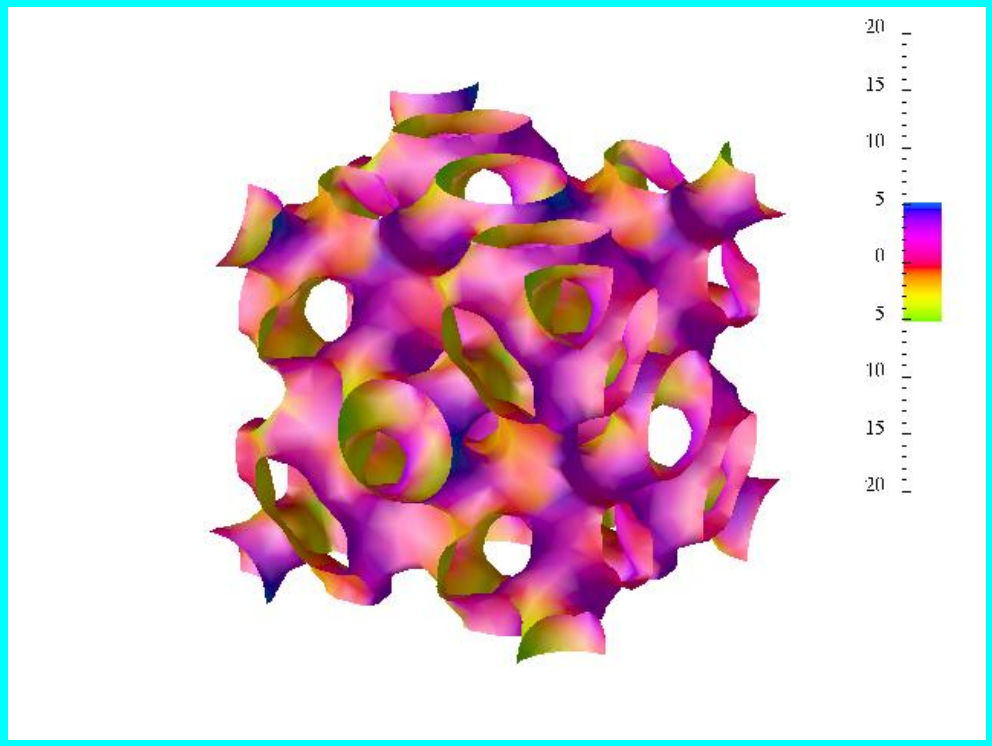
20
15
10
5
0
5
10
15
20

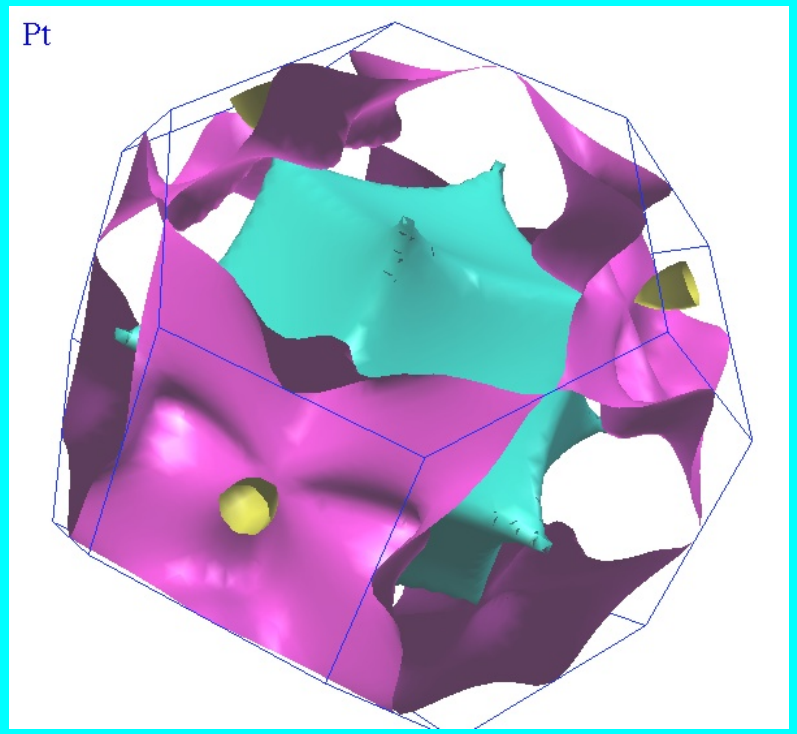
Pt

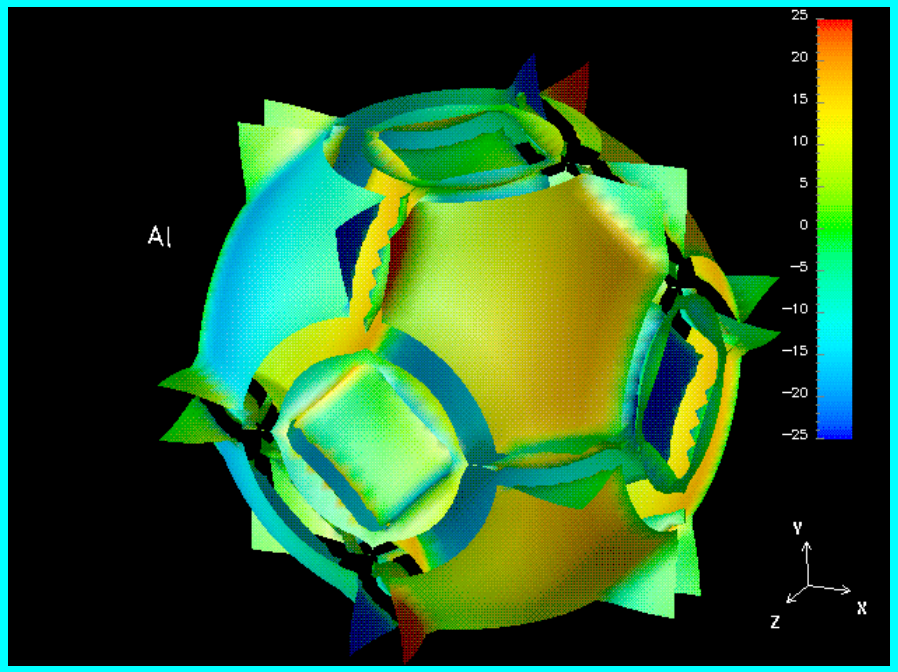
Al
25
20
15
10
5
0
−5
−10
−15
−20
−25
Y
Z
X

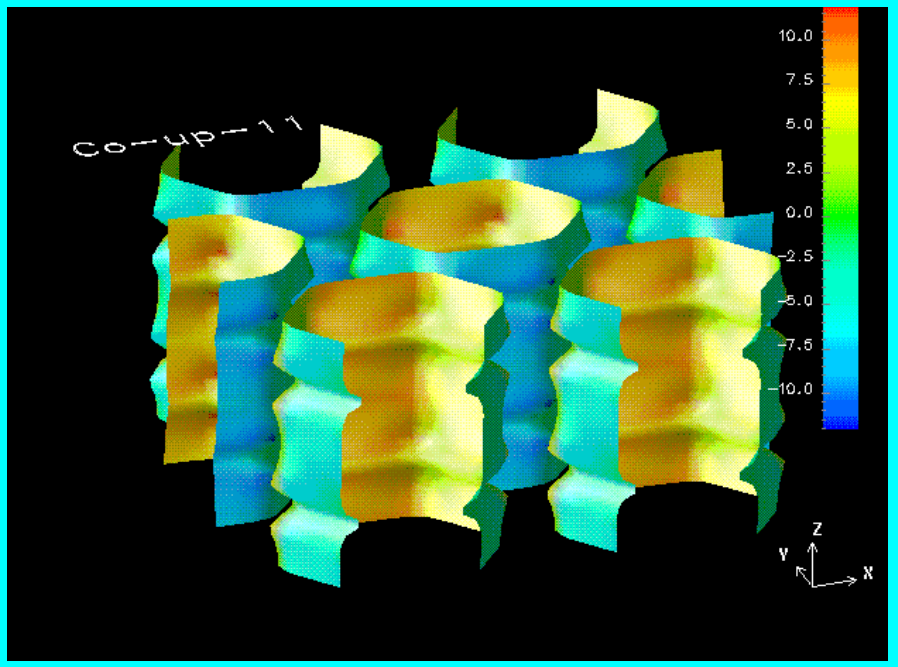
Co−up−11
10.0
7.5
5.0
2.5
0.0
−2.5
−5.0
−7.5
−10.0
Z
Y
X

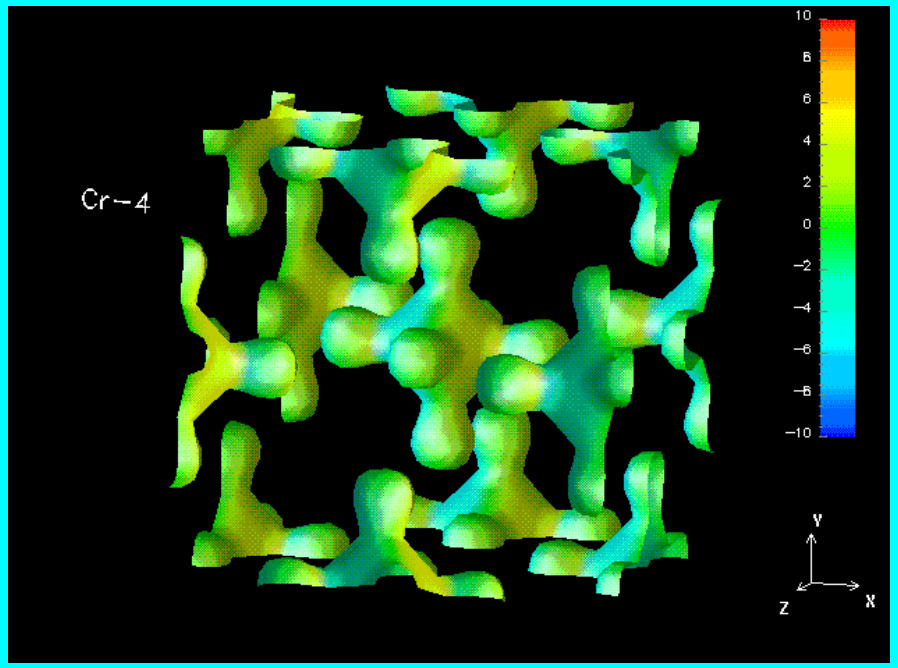
Cr−4
10
8
6
4
2
0
−2
−4
−6
−8
−10
Y
Z
X

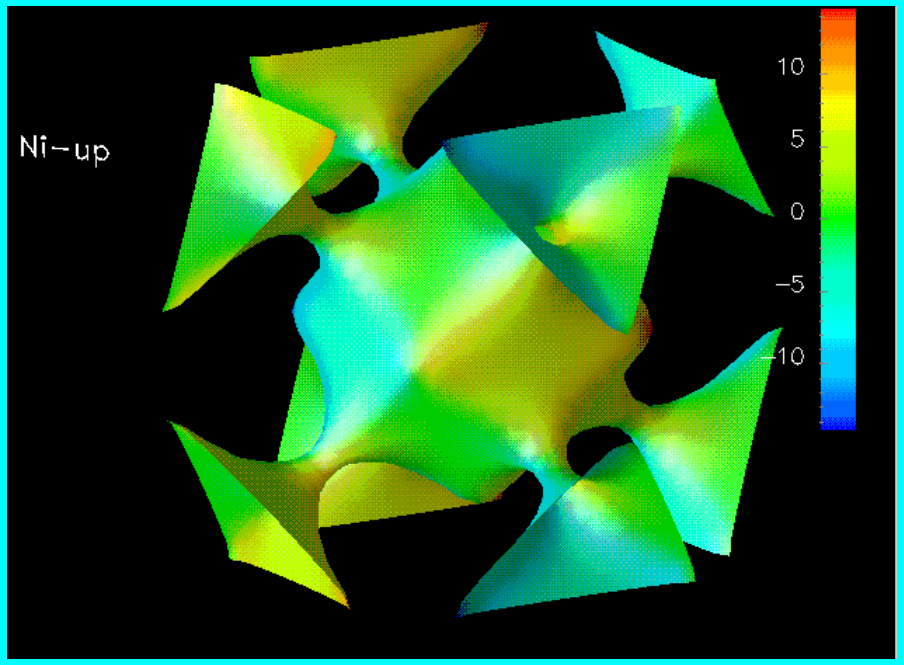
Ni−up
10
5
0
−5
−10

Zwei Methoden zur Messung der effektiven Masse: Wärmekapazität

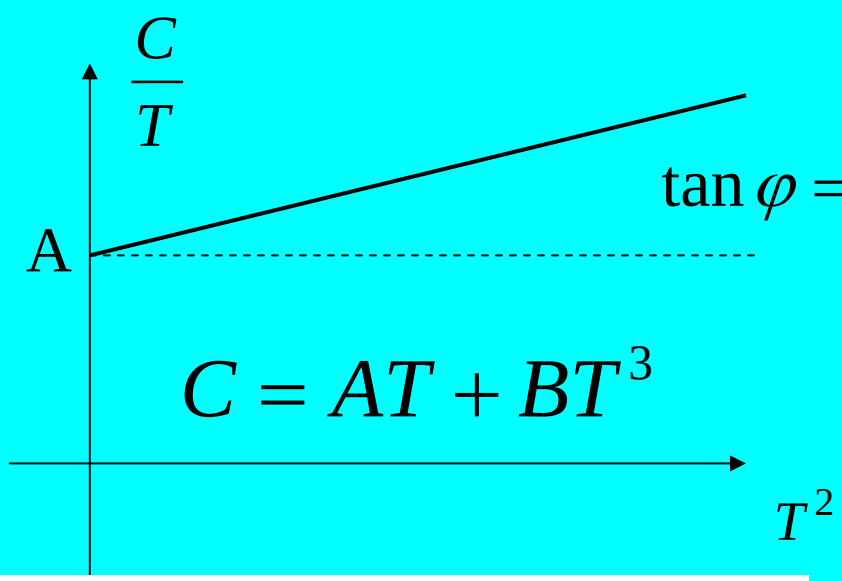

$$E = 2V \int \epsilon(p) n(\epsilon_p) \frac{d^3p}{(2\pi\hbar)^3}$$

$$C = V^{-1} \left(\frac{\partial E}{\partial T}\right)_V = 2 \int \epsilon(p) \left(\frac{\partial n(\epsilon_p)}{\partial T}\right) \frac{d^3p}{(2\pi\hbar)^3}$$

$$C = \frac{\pi^2}{3} \rho(0) T = \gamma T$$

$$\gamma = \frac{p_F m^*}{3\hbar^3}$$

$$\rho(0) = \frac{p_F m^*}{\pi^2 \hbar^3}$$

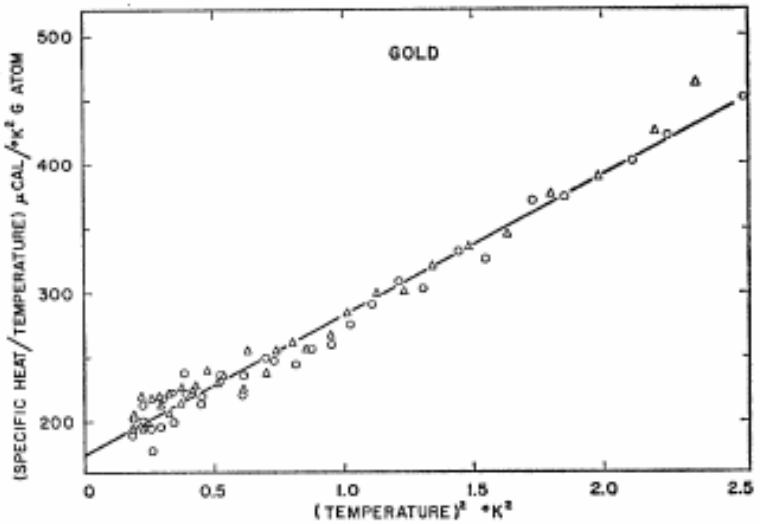

FIG. 1. Plot of (specific heat/temperature) versus (temperature²) for gold.

	N/V $[cm^{-3}]$	ϵ_F [eV]	T_F [K]	m^*/m
Li	4.6×10^{22}	4.7	5.5×10^4	2.3
Na	2.5	3.1	3.7	1.3
K	1.34	2.1	2.4	1.2
Cu	8.5	7.0	8.2	1.3
Ag	5.76	5.5	6.4	1.1
Au	5.9	5.5	6.4	1.1

Zwei Methoden zur Messung der effektiven Masse:

de Haas-van Alphen Effekt (dHvA)

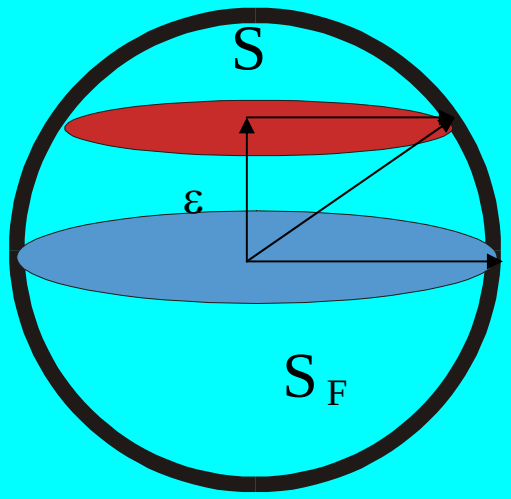

$$M \approx T\sqrt{\frac{2e\hbar}{\pi^3 cH}}\sum_m S_m \left|\frac{\partial^2 S_m}{\partial p_z^2}\right| \exp\left(-\frac{2\pi^2 T c m^*}{e\hbar H}\right) \sin\left(\frac{cS_m}{e\hbar H} \pm \frac{\pi}{4}\right) \cos\left(\frac{\pi m^*}{m}\right)$$

$$m^* = \frac{1}{2\pi}\frac{\partial S}{\partial \epsilon}$$

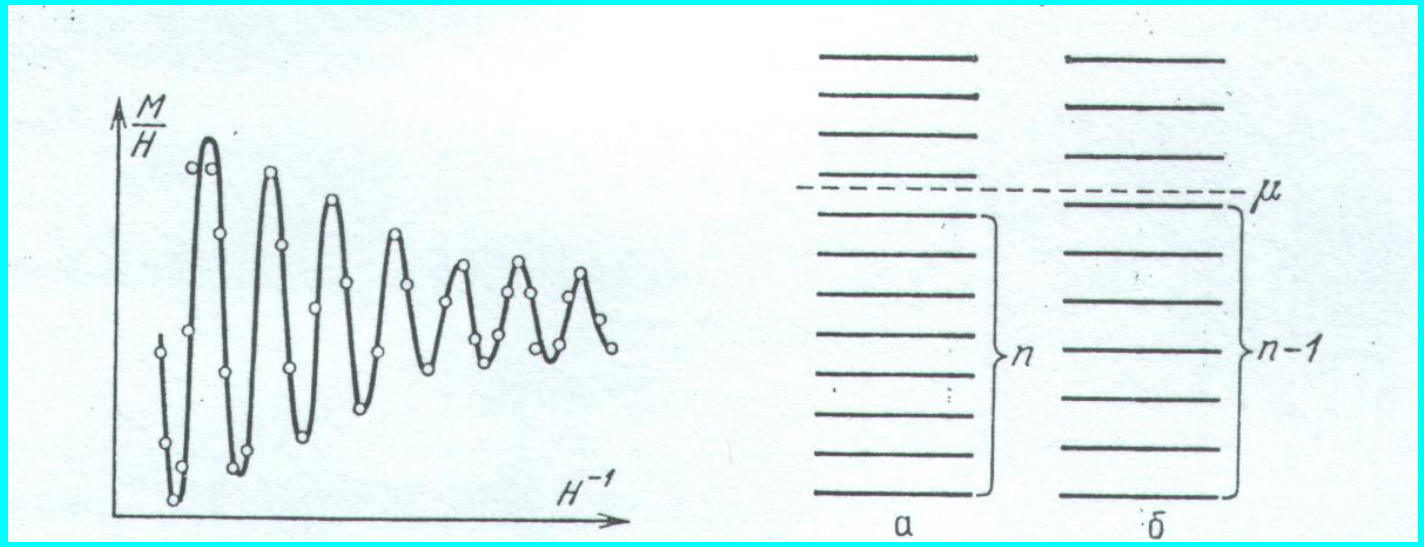

Schwer-Fermionen Materialen

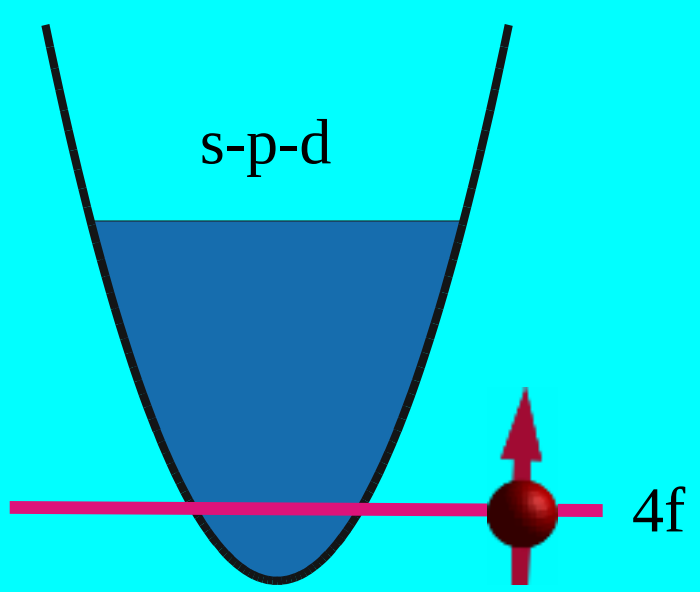

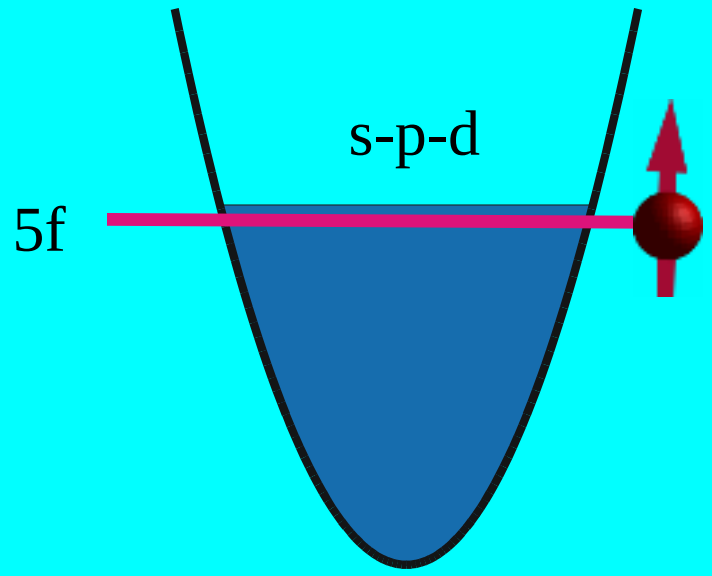

System	γ_0 (J/K^2mol)	T_F K	m^*/m	T_c K	T_K K
$CeCu_6$	1.6	300	500	-	5
$CeAl_2$	0.14	4000	42	-	3.9
$CeCu_2Si_2$	1.1	350	450	0.8	10
$CeRu_2Si_2$	0.35	1200	100	-	20
UBe_{13}	0.72	700	260	-	8
UPt_3	0.42	1100	180	5	80
UCd_{11}	1.42	400	425	5	-
U_2Zn_{17}	0.42	1100	180	10	-

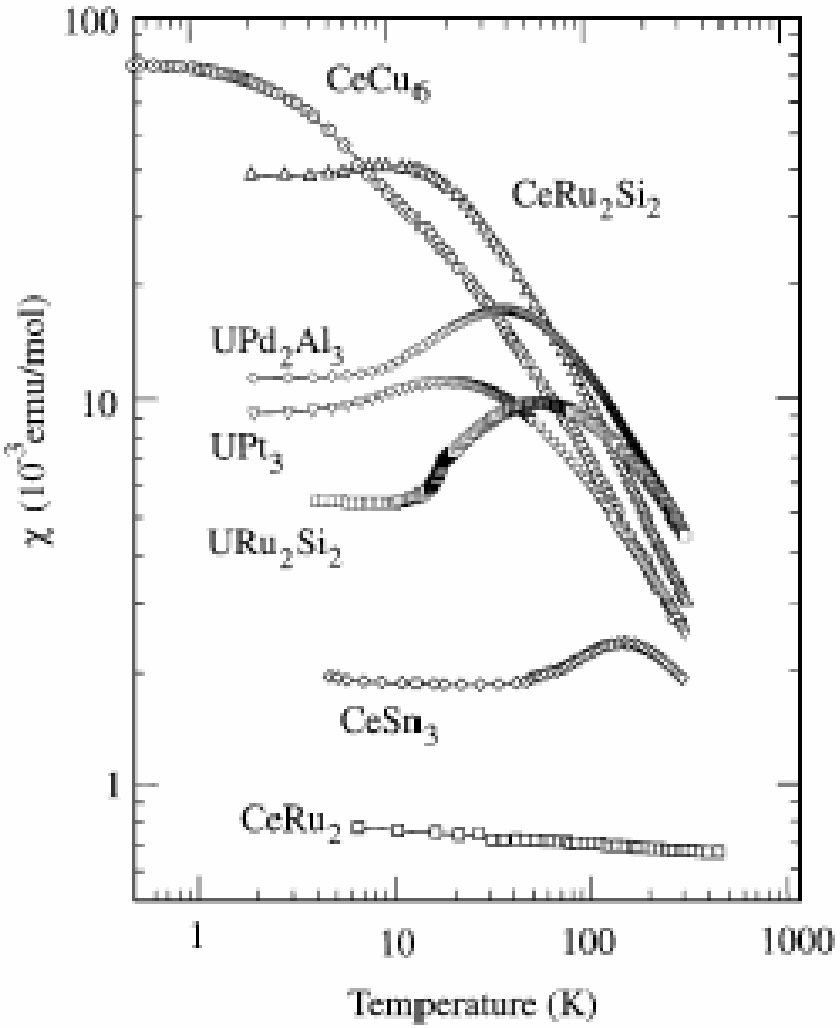

Fig. 2. Temperature dependence of the magnetic susceptibility of cerium and uranium compounds.

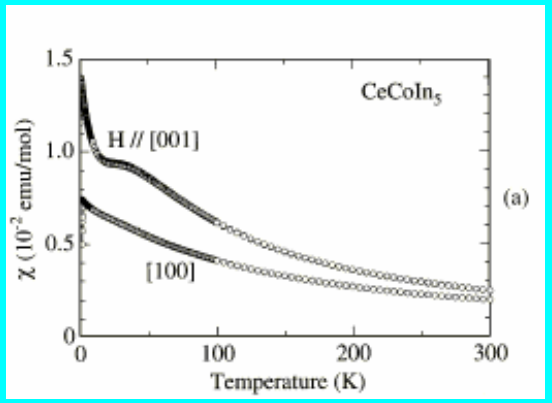

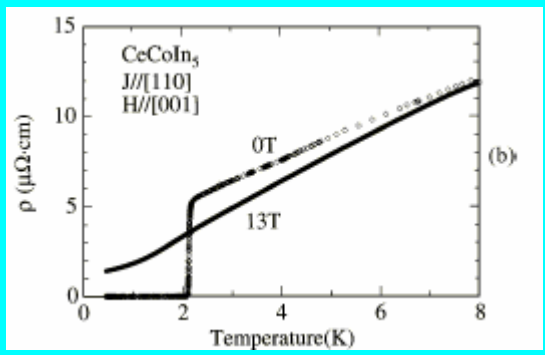

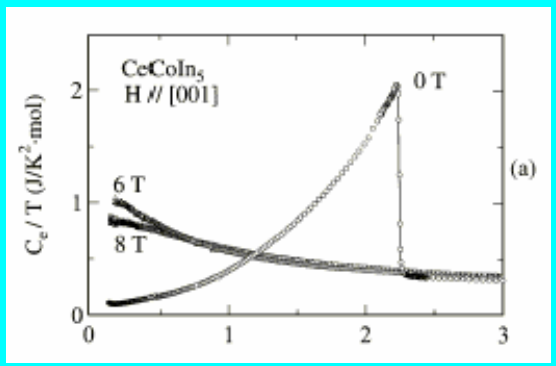

$$C_s = (2\pi/3)n_s T/T^*, \qquad \chi_s = (4/\pi)\mu_B^2 n_s/T^*, \qquad \rho = \rho_0 + \rho_J[1+(T/T^*)^2]$$

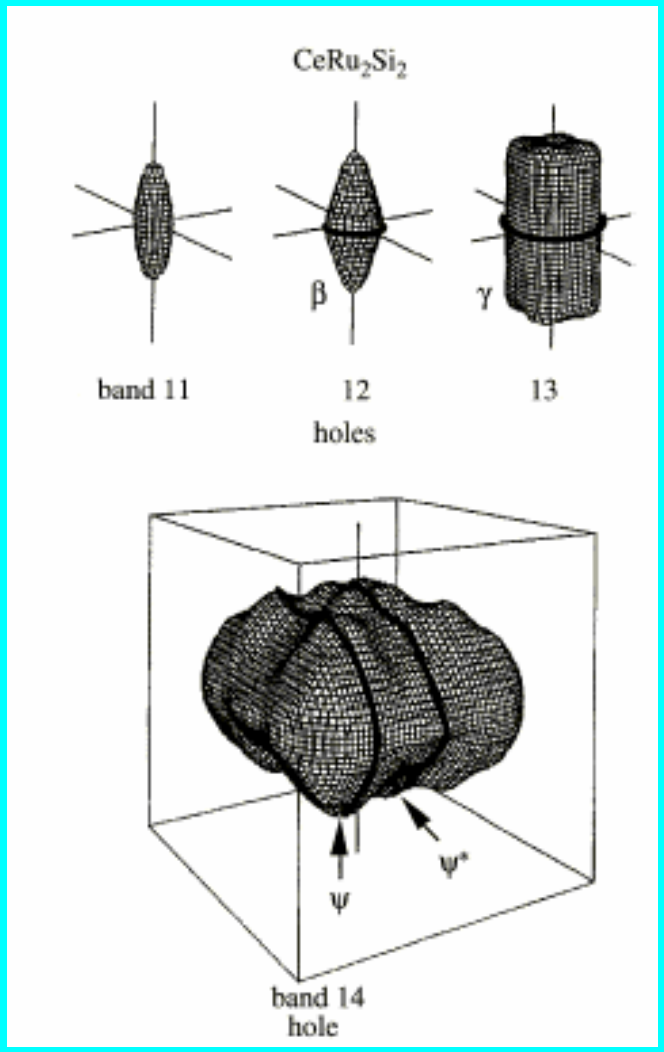

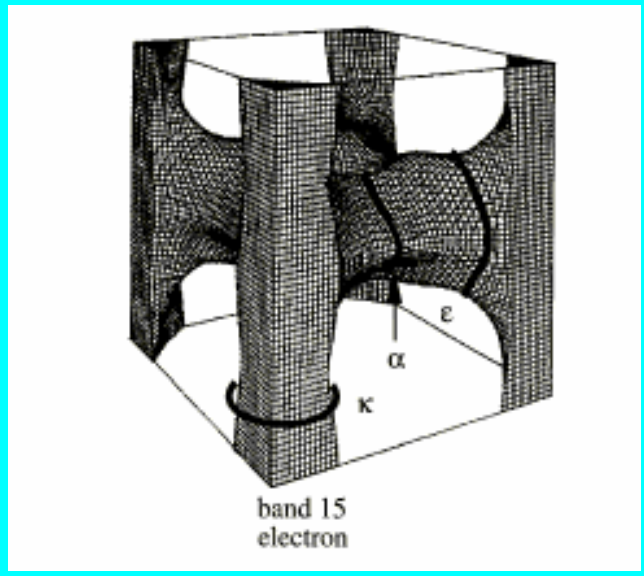

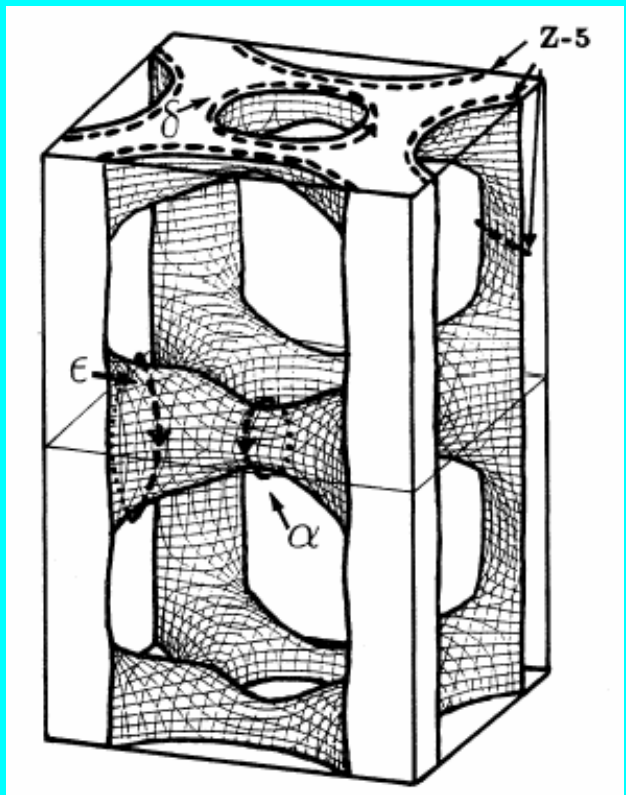

Y.Onuki, R.Settai, Physica B 300, 61 (2001)

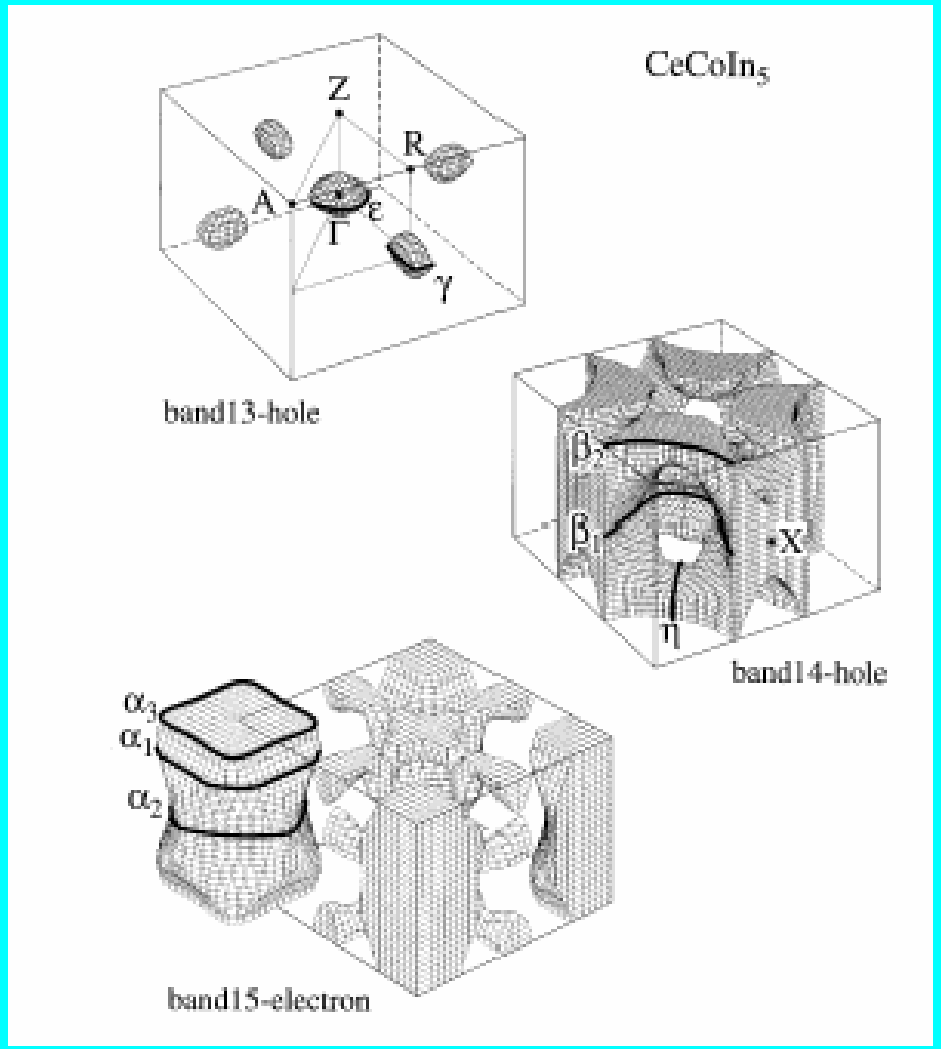

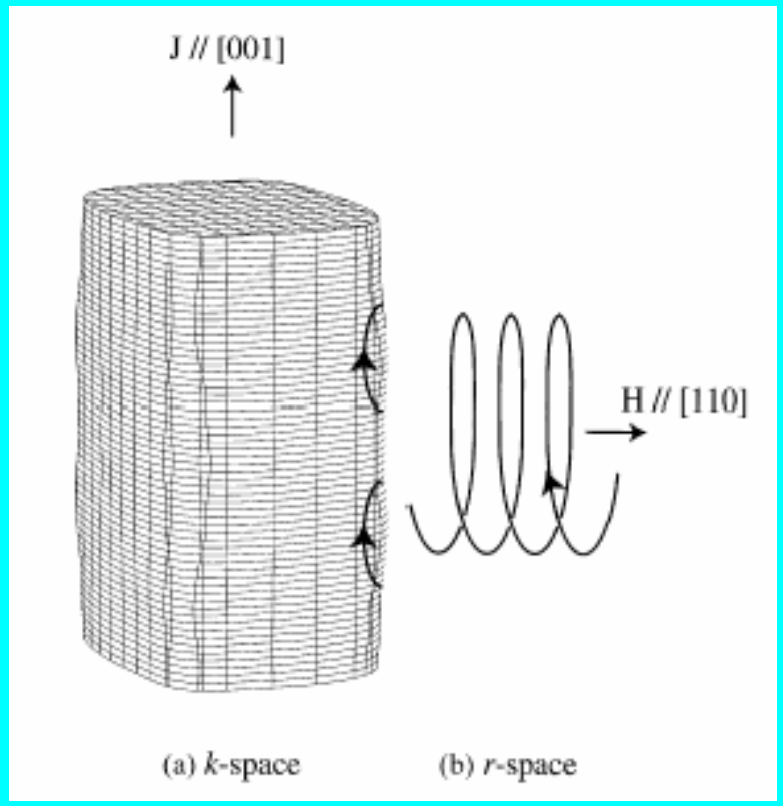

Y.Onuki, R.Settai, Physica B 300, 61 (2001)

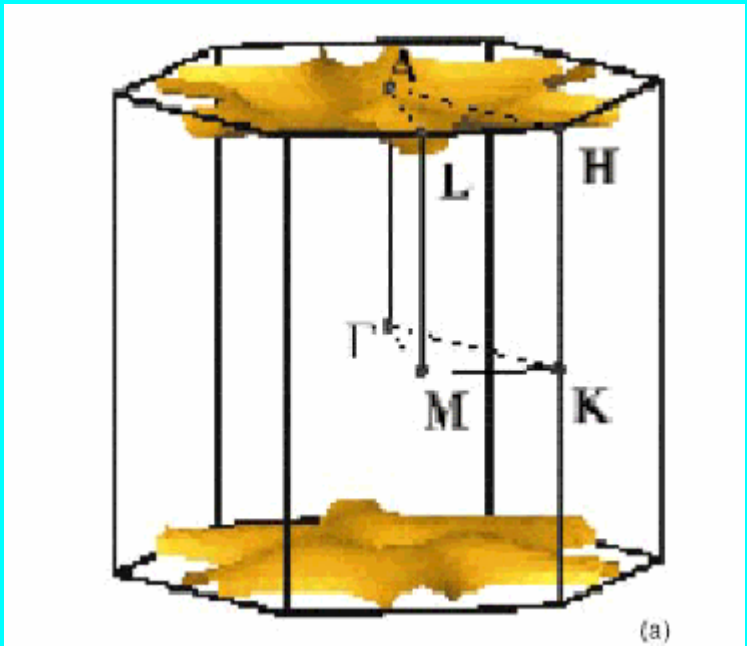

G. Zwicknagl, et al, Phys.Rev.B 65, 081103R (2002)

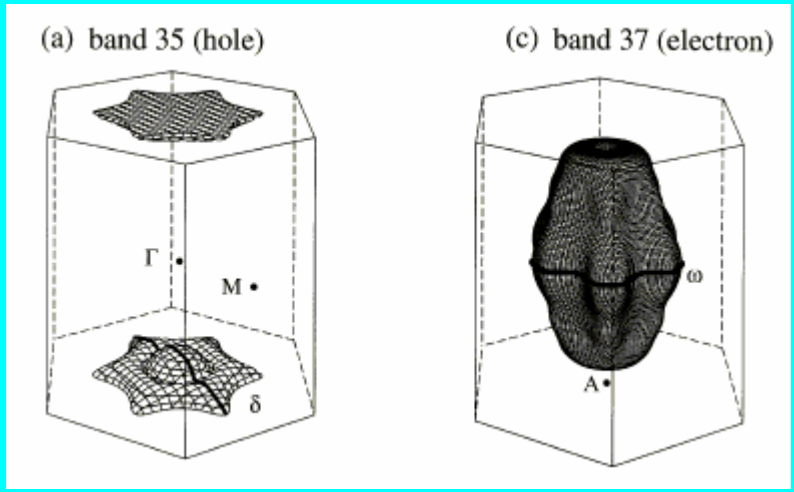

Y.Onuki, R.Settai, Physica B 300, 61 (2001)

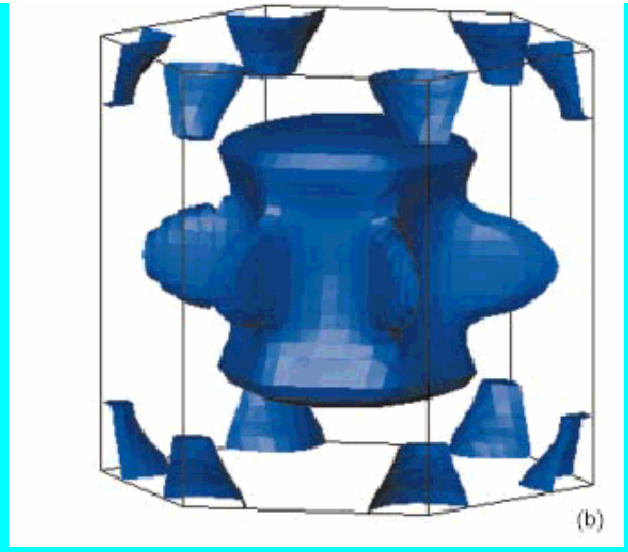

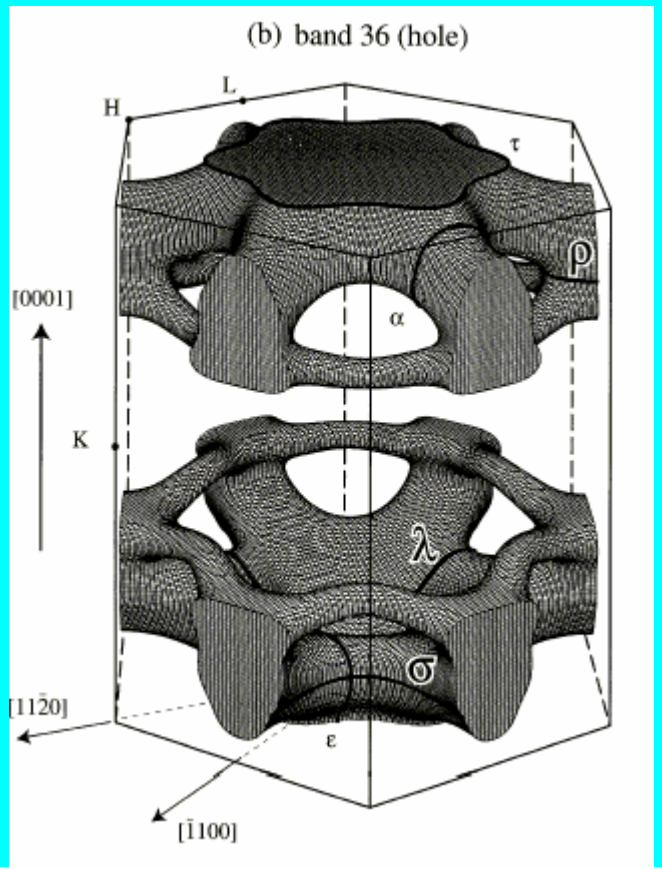

Nicht-Fermi-Flüssigkeit und quanten ktitisches Regime

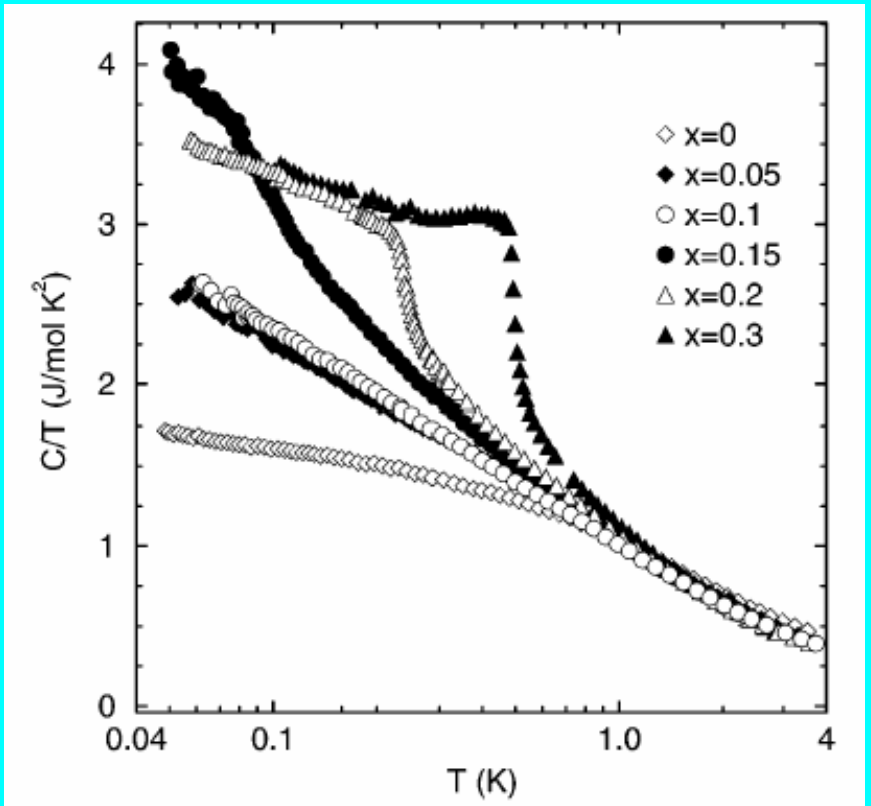

FIG. 2. The specific heat C/T of $CeCu_{6-x}Au_x$ (from [7]) on a logarithmic scale.

A.Rosch et all, Phys.Rev.Lett 79, 159 (1997)

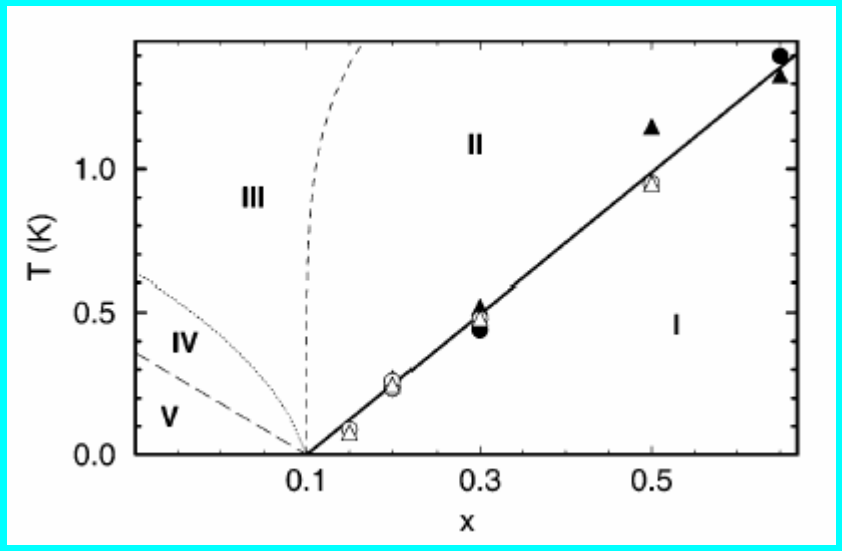

M.B.Maple et al. JLTP 99, 223 (1995)

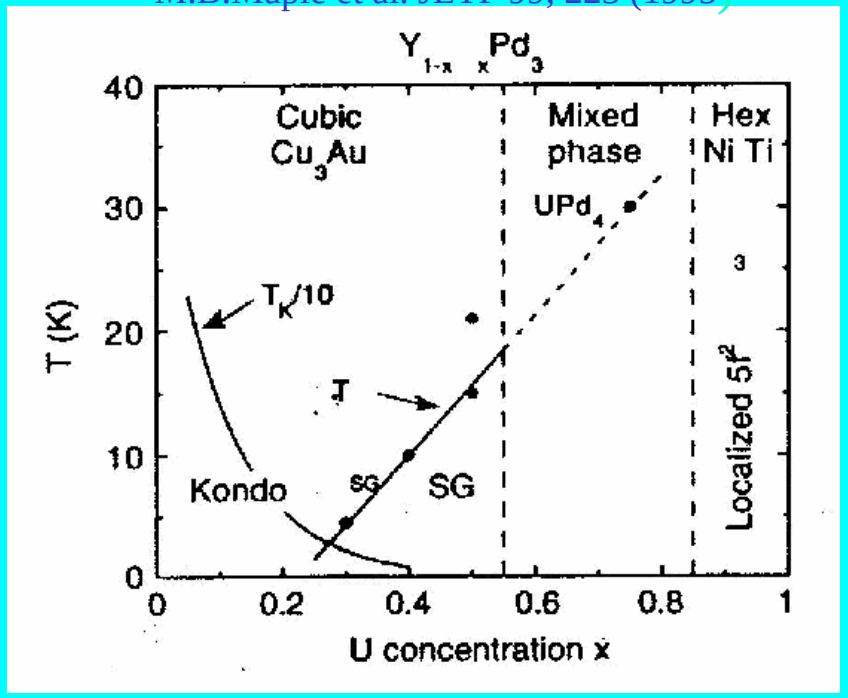

Fragen

- Warum sind die Quasiteilchen so schwer?
- Warum unterscheiden sich die Massen aus Wärmekapazitäts- und dHvA-Messungen?
- Warum ist die Fermi-Fläche so groß trotz großer Massen?
- Was ist der Grund für das quanten-kritische Verhalten?

Das Modell

$$H = \sum_k \varepsilon(k) c^+_{k,\sigma} c_{k,\sigma} + J \sum_i \vec{S}_i \vec{s}_i + \sum_{ij} I_{ij} \vec{S}_i \vec{S}_j$$

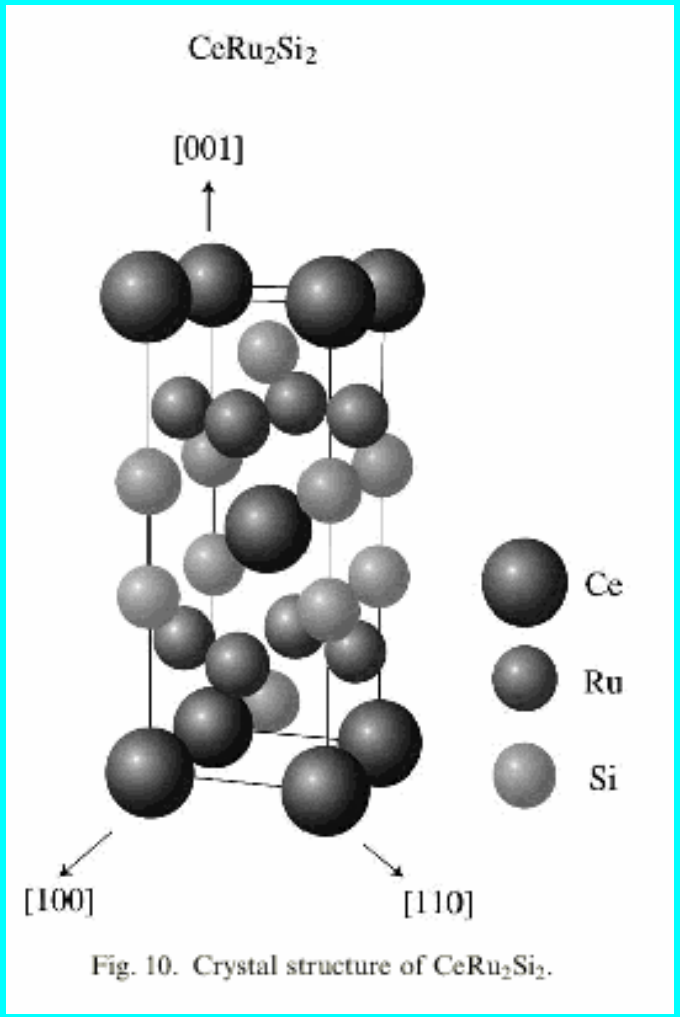

Fig. 10. Crystal structure of $CeRu_2Si_2$.

$$H_{Kondo} = J \sum_i \vec{S}_i \vec{s}_i$$

$$H_{RKKY} = \sum_{i,j} I_{ij} \vec{S}_i \vec{S}_j$$

Kondo-Effekt

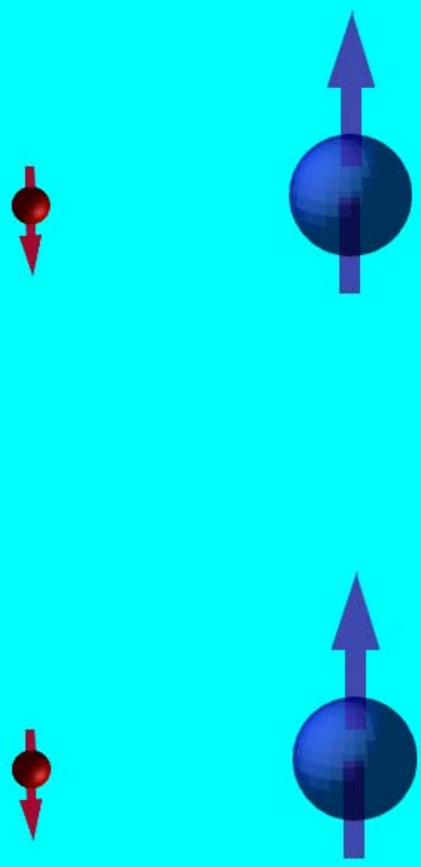

$$H_{Kondo} = J \sum_i \vec{S}_i \vec{s}_i$$

$$\rho = \rho_v + c_m a \ln(\mu/T) + bT^5$$

Widerstand bei niedrigen Temperaturen

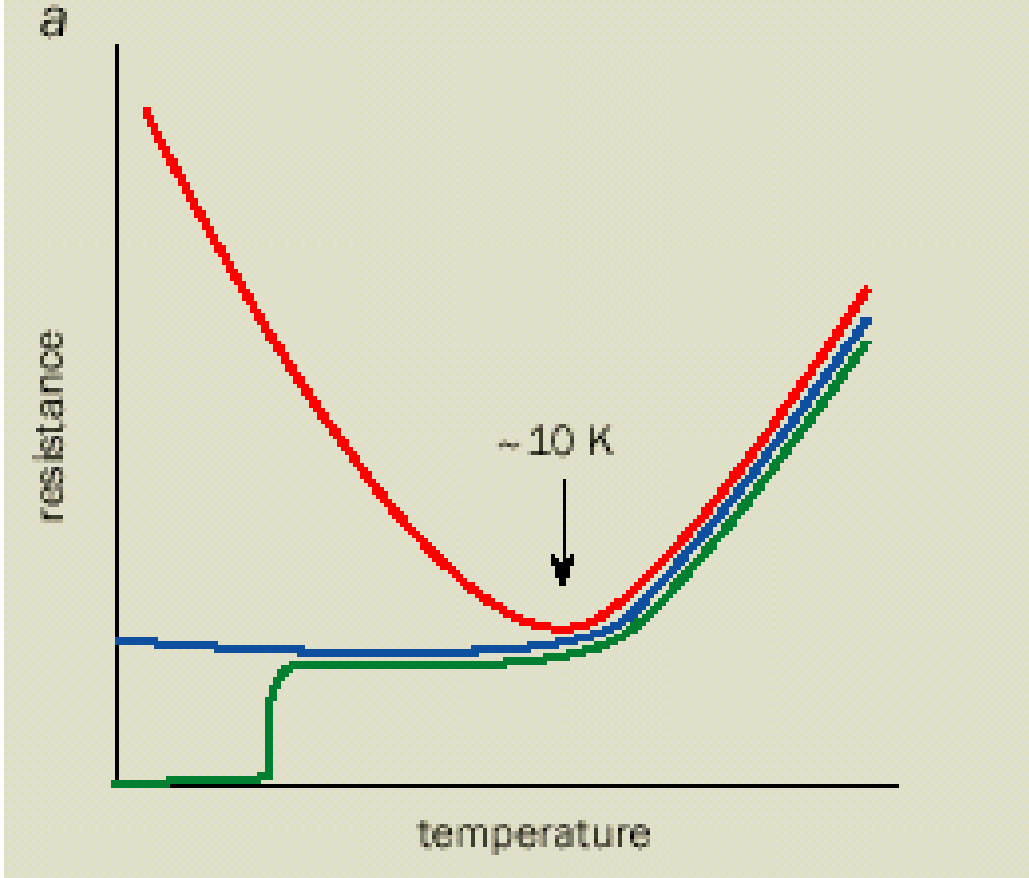

$$\rho = \rho_v + c_m a \ln(\mu/T) + bT^5$$

Renormierung der Kondo Wechelwirkung

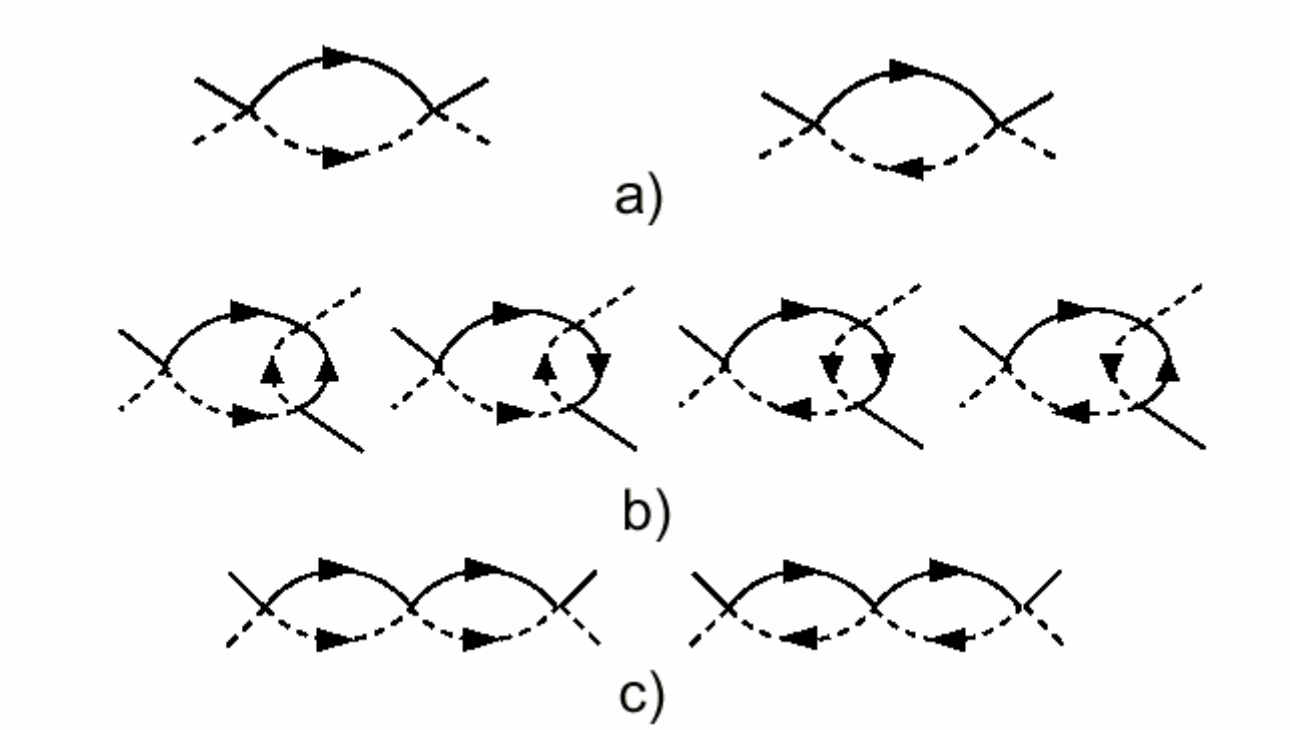

$$\bar{J} = \frac{J}{1 - \rho(0) J \ln\left(\frac{\epsilon_F}{\max[T, \omega]}\right)}$$

Kondo-Abschirmung

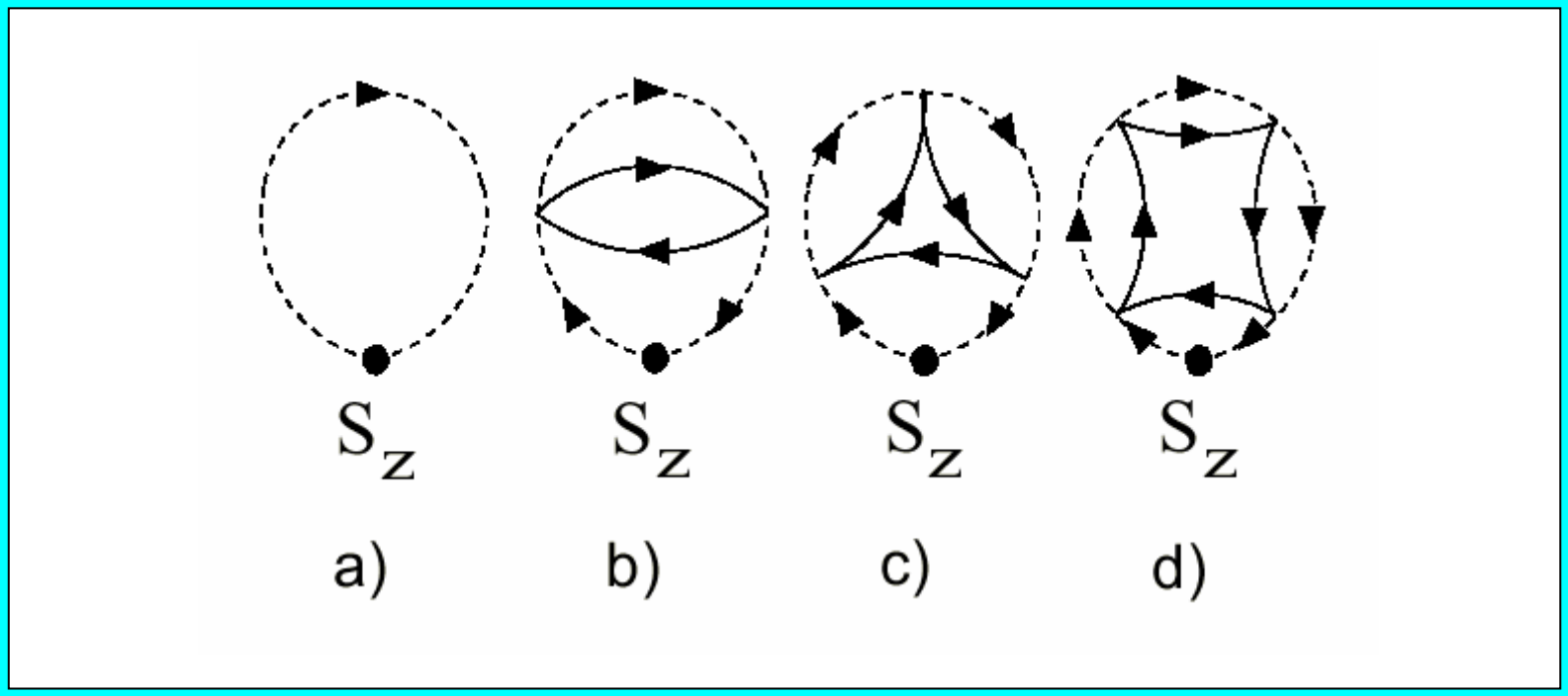

$$\mathcal{M}(H) = S(g\mu_B)\tanh\left(\frac{H\beta}{2}\right)\left[1 - \frac{1}{\ln(T/T_K)} - \frac{\ln(\ln(T/T_K))}{2\ln^2(T/T_K)} + \ldots\right]$$

Kondo Wolke

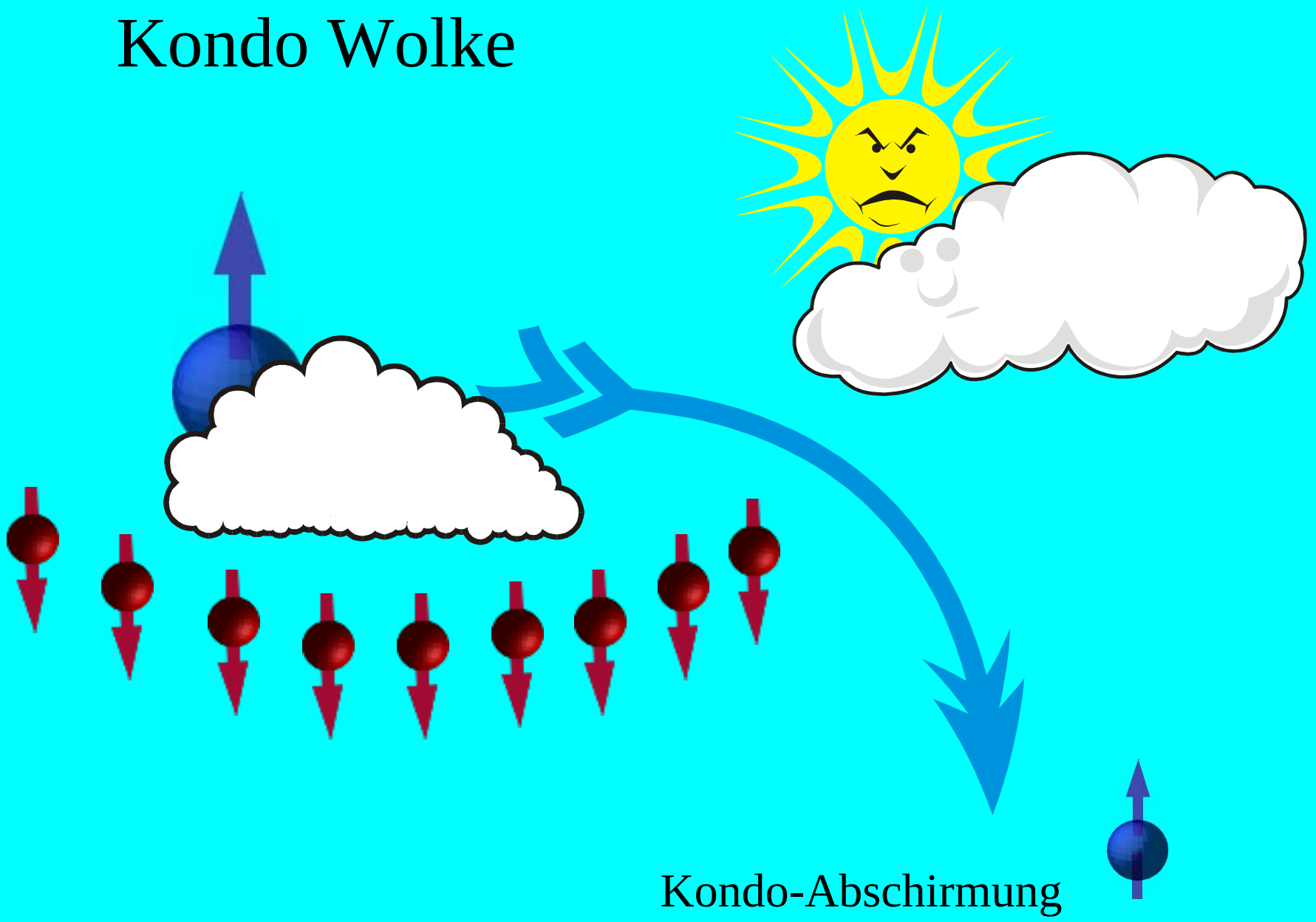

Kondo-Abschirmung

Exakte Lösung des single-impurity Kondo Problem

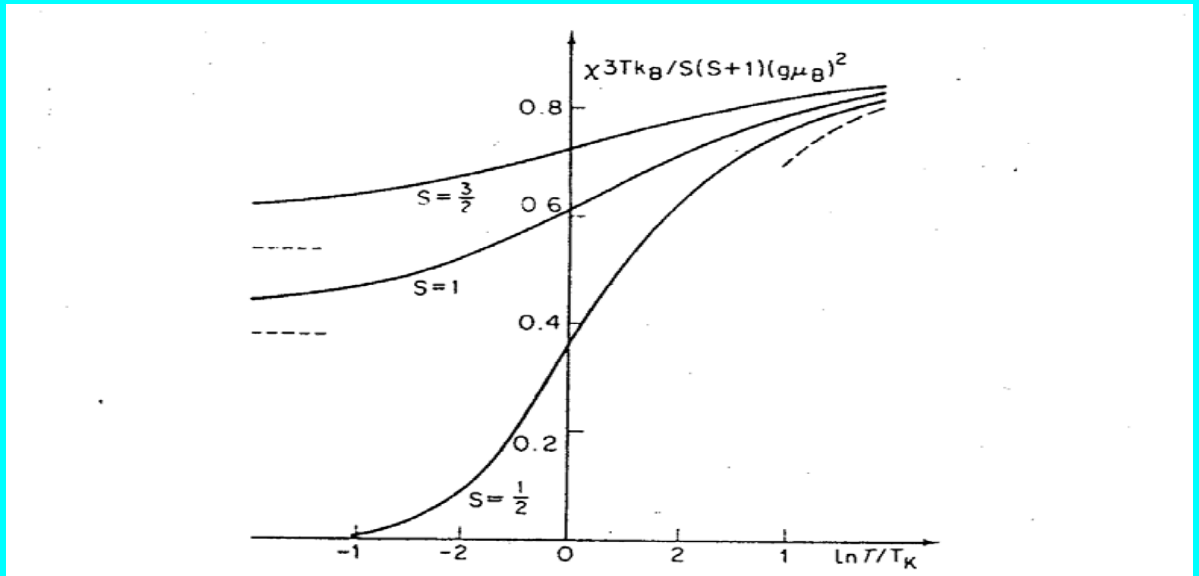

The $3k_B T\chi_s/S(S+1)(g\mu_B)^2$ versus $\ln T/T_K$ plot for $S=1/2$, 1, 3/2 impurities. The dashed line in the right-hand side of the figure is the high-temperature asymptotic behaviour: $3T\chi_s/S(S+1)\to 1-1/(\ln T/T_K)$. The dashed lines in the left-hand side are the low-temperature ones: $3T\chi_s\to S^2-1/4$ (after Melnicov 1982 a).

A.M.Tsvelik and P.Wiegmann Adv.Phys. 32, 453 (1983)

$$\chi_0(T) = \frac{S(S+1)(g\mu_B)^2}{3T}(1 - \frac{1}{\ln(T/T_k)} + ...)$$

Ruderman-Kittel-Kasuya-Yosida (RKKY) Wechselwirkung

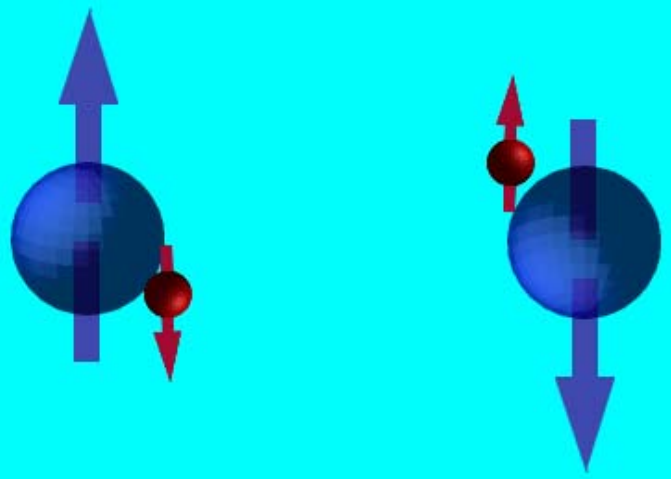

$$H_{RKKY} = \sum_{i,j} I_{ij} \vec{S}_i \vec{S}_j$$

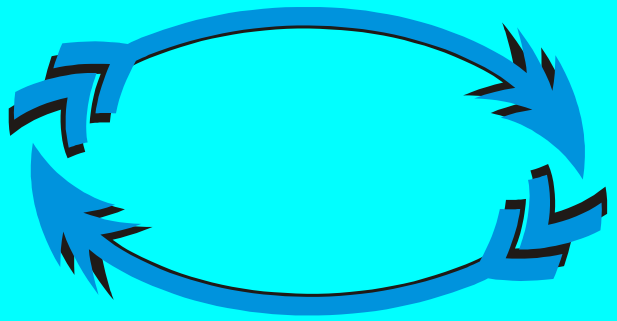

$$I_{RKKY} = 2\left(\frac{J}{n}\right)^2 \sum_{p,p'} \frac{n_{\mathbf{p}}(1-n_{\mathbf{p}'})}{\epsilon_{\mathbf{p}} - \epsilon_{\mathbf{p}'}}$$

$$I_{RKKY}(q) = -\frac{m^* p_F}{4\pi^2\hbar^3}\left(\frac{J}{n}\right)^2 \left[1 + \frac{(2p_F)^2 - q^2}{4p_F q} \ln\left|\frac{2p_F - q}{2p_F + q}\right|\right]$$

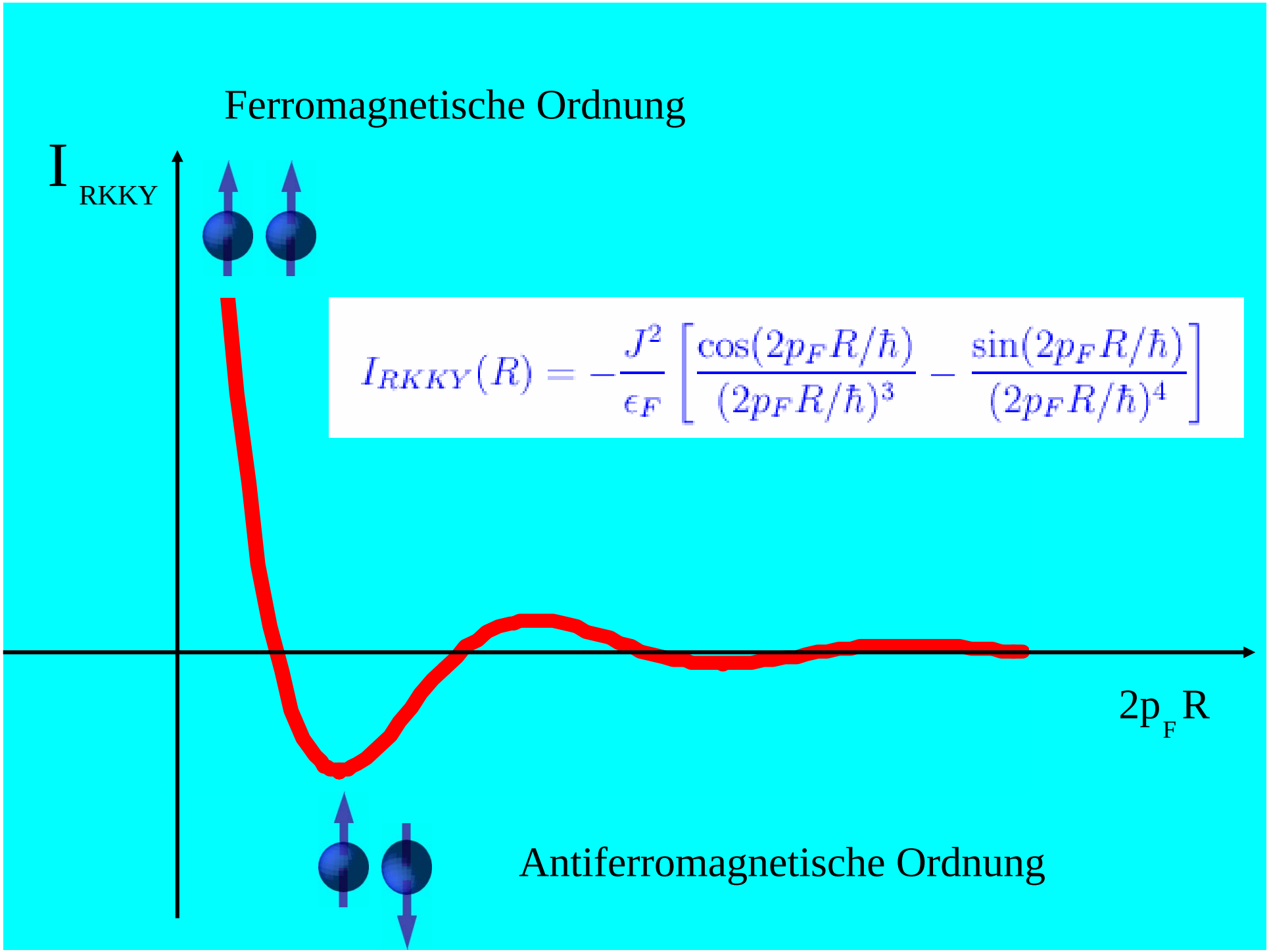
Ferromagnetische Ordnung
I RKKY
$I_{RKKY}(R) = -\frac{J^2}{\epsilon_F}\left[\frac{\cos(2p_F R/\hbar)}{(2p_F R/\hbar)^3} - \frac{\sin(2p_F R/\hbar)}{(2p_F R/\hbar)^4}\right]$
2p F R
Antiferromagnetische Ordnung

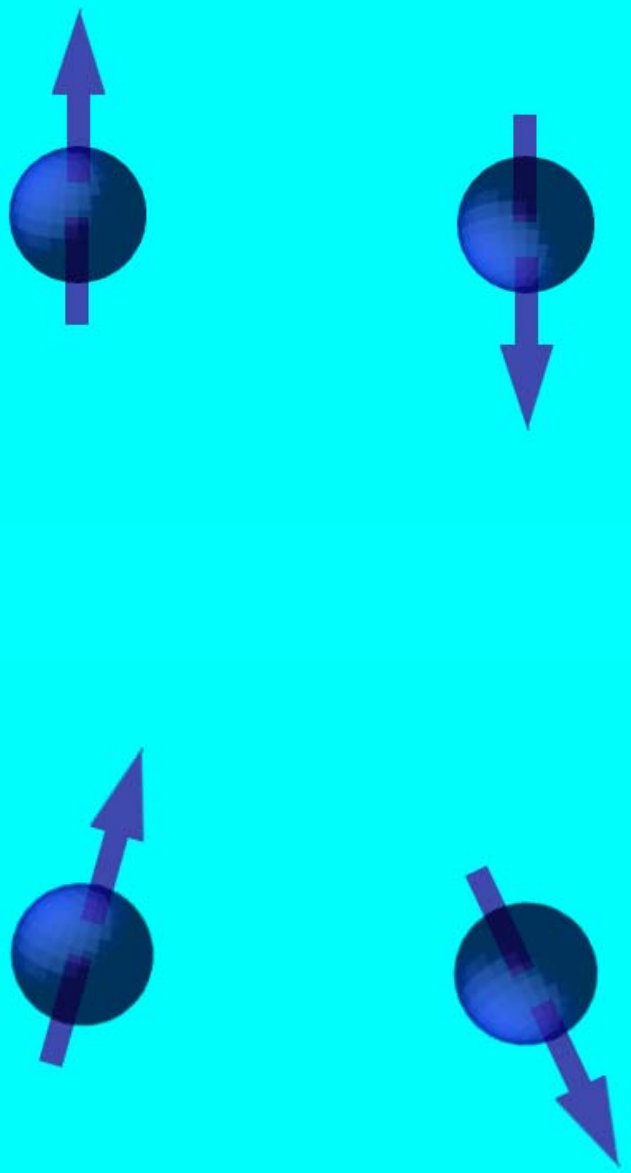

Antiferromagnetische Ordnung

$$T > T_c$$

$$\mathcal{N} = \tanh\left(\frac{I_Q \mathcal{N}}{2T}\right)$$

$$T < T_c$$

$$\mathcal{N} = \tanh\left(\frac{I_Q \mathcal{N}}{2T}\right)\left[1 - \frac{a_N}{\ln(T/T_K)}\frac{\cosh^2(\beta I_Q \mathcal{N}/2)}{\cosh^2(\beta I_Q \mathcal{N})}\right]$$

M.Kiselev et al, Phys.Rev. B 65, 184410 (2002)

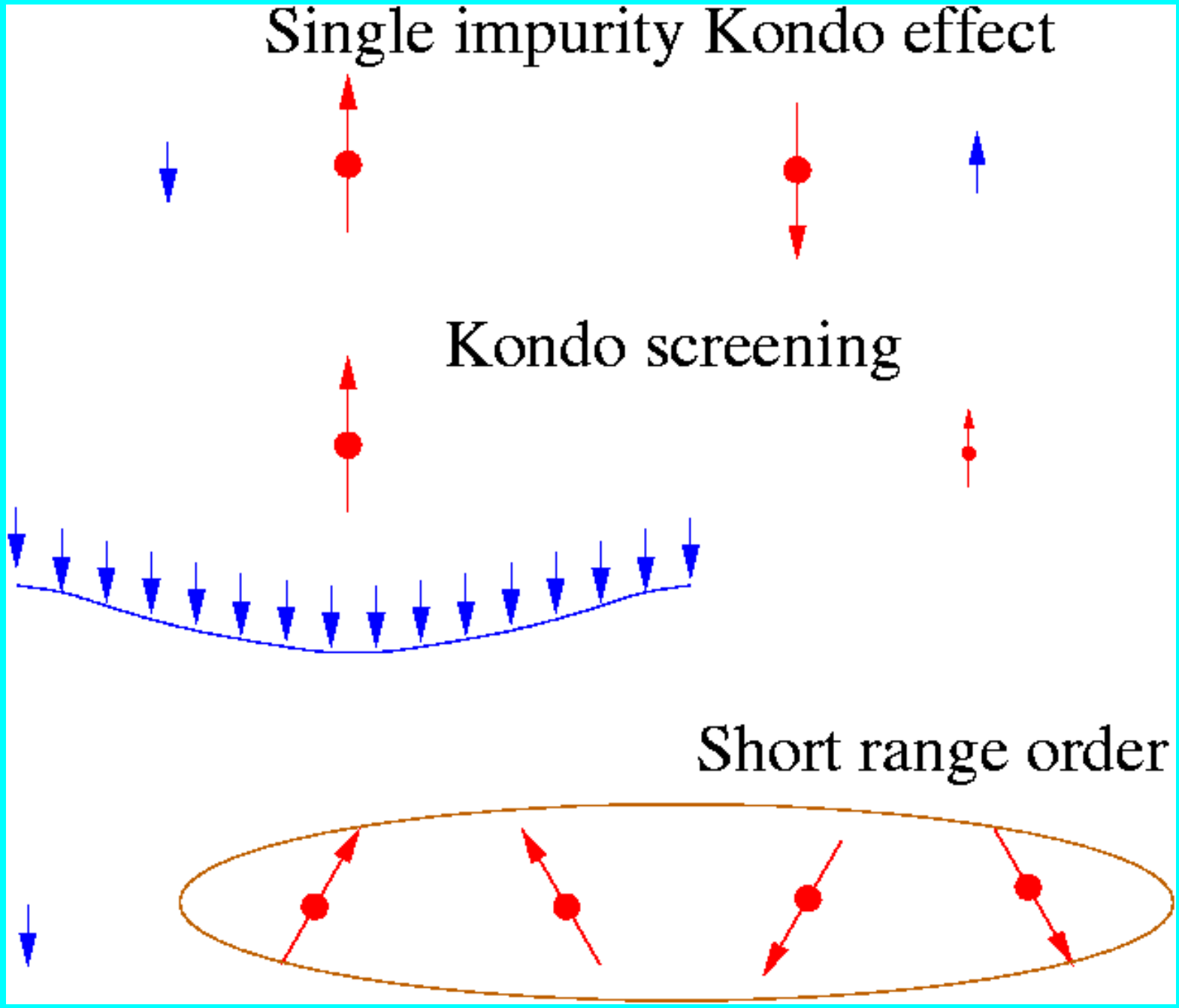
Single impurity Kondo effect
Kondo screening
Short range order

Spin Flüssigkeit

Resonating Valence Bonds

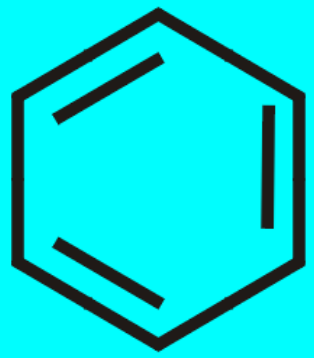

$$\Delta = -\sum_{\mathbf{q}} \nu(\mathbf{q}) \tanh\left(\frac{I_{\mathbf{q}}\Delta}{T}\right)$$

$$\Delta = -\sum_{\mathbf{q}} \nu(\mathbf{q}) \left[\tanh\left(\frac{I(\mathbf{q})\Delta}{T}\right) + a_{sl}\frac{I_{\mathbf{q}}\Delta}{T\ln(T/T_K)}\right]$$

M.Kiselev et al, Phys.Rev. B 65, 184410 (2002)

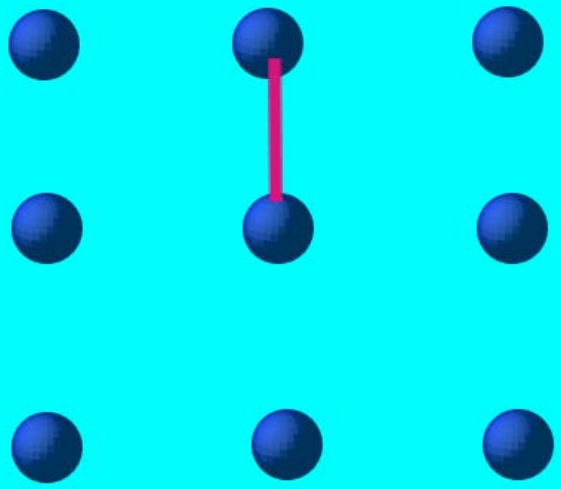

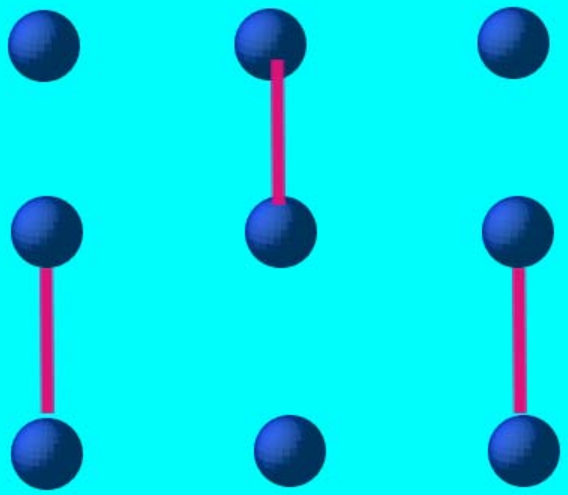

Die Methode

We apply the decoupling (5) and (11) to KLM with quenched disorder. We assume that $T_{SG} \sim T^*$, where T^* stands for T_K in a lattice.

$$< Z^n >_{av} = \exp\left(-\frac{1}{4}(\beta I)^2 N(n\tilde{q}^2 + n(n-1)q^2) + \right.$$

$$\left. + \sum_i \ln\left[\prod \int D[\varphi^a, \psi^a] \int_z^G \int_{y^a}^G \exp(\mathcal{A}[\varphi^a, \psi^a, y^a, z])\right]\right)$$

where $\mathcal{A}[\varphi^a, \psi^a, y^a, z] = \sum_{a,\sigma} \bar{\varphi}^a_\sigma \left[\mathcal{G}_a^{-1} - \sigma H(y^a, z)\right] \varphi^a_\sigma - \frac{2}{J}\sum_\omega |\psi^a|^2$ and the inverse GF for Popov-Fedotov spin-fermions

$$\mathcal{G}_a^{-1} = i\omega_1 \delta_{\omega_1,\omega_2} - T\sum_\epsilon \psi_i^{a*}(\epsilon_l + \omega_1) G_0(-i\nabla_i, \epsilon_l)\psi_i^a(\epsilon_l + \omega_2)$$

Thus, we mapped KL problem with disorder onto effective one-site interacting Kondo system coupled with external local replica-dependent magnetic field. To take into account dynamical effects due to the Kondo scattering we include H into bare spin-fermion GF [10].

$$\mathtt{Tr}\ln\left(\mathcal{G}_a^{-1} - \sigma H\right) = \ln\left(2\cosh(\beta H)\right) + \mathtt{Tr}\sum_{m=1}^{\infty} \frac{(-1)^{m+1}}{m}\left(\mathcal{G}^a_{0\sigma}\Sigma(\psi^a)\right)^m$$

The effective action for KLM in one loop approximation is given by

$$\mathcal{A}[\psi^a, H] = \ln\left(2\cosh(\beta H)\right) - \frac{2}{J}\sum_n \left[1 - J\Pi(i\Omega_n, H)\right]|\psi^a|^2 \qquad (2)$$

The free energy and SG order parameter are determined by

$$\beta f(\tilde{q}, q) = \frac{1}{4}(\beta I)^2\left(\tilde{q}^2 - q^2\right) - \int_z^G \ln\left(\mathcal{F}(q, \tilde{q}, z)\right)$$

$$\frac{1}{2}(\beta I)^2(\tilde{q}, q) = \pm\int_z^G \frac{\partial \ln \mathcal{F}}{\partial(\tilde{q}, q)}), \quad \mathcal{F} = \int_y^G \frac{2\cosh(\beta H(y,z))}{1 - J\Pi(0, H(y,z))} \qquad (3)$$

In the vicinity of SG phase transition point Eq.(17) reads:

$$\tilde{q} = 1 - \frac{2c}{\ln(T/T^*)} + O\left(\frac{1}{\ln^2(T/T^*)}\right)$$

$$q = \int_z^G \tanh^2\left(\frac{\beta I z\sqrt{q}}{1 + 2c(\beta I)^2(\tilde{q} - q)/\ln(T/T^*)}\right) + O\left(\frac{q}{\ln^2(T/T^*)}\right)$$

Taking the limit $q \to 0$ we estimate the temperature of SG transition $(T_{SG}/T^0_{SG})^2 = 1 - 4c/\ln(T^0_{SG}/T^*) - ... < 1$, $T^0_{SG} = I$, $c \sim 1$.

We decouple the Kondo term in (1) by four component field $\Upsilon_i = (\psi_i, \vec{\Phi}_i)$ and integrate over all conduction electrons

$$\mathcal{A}[a, \Upsilon] = \mathcal{A}_0[\psi] + \mathcal{A}[\vec{\Phi}] + \sum_i \sum_{(\omega_n)} \bar{a}_\sigma(\omega)\mathcal{G}_{\sigma\sigma'}a_{\sigma'}(\omega)$$

$$\mathcal{G}^{-1}_{\sigma\sigma'} = \delta_{\sigma\sigma'}\left[(i\omega_1 - \frac{\sigma g h}{2})\delta_{\omega_1,\omega_2} - T\sum_\epsilon G_i(\epsilon)\psi_i^*(\epsilon + \omega_1)\psi_i(\epsilon + \omega_2)\right] - \vec{\sigma}^a\vec{\Phi}_i$$

We incorporate the "condensate" part of Φ^z into bare GF of spin-fermions as a local external effective magnetic field. As a result,

$$\delta\mathcal{A}^{(1)}_{eff}[\psi] = -2\sum_{\vec{k}}\left[\frac{1}{J} - \Pi(0, \mathcal{N})\right]\psi^2_{\vec{k}}(0) - 2\sum_{\vec{k}}\sum_{\Omega\neq 0}\left[\frac{1}{J} - \Pi(\Omega_n, \mathcal{N})\right]\psi^2_{\vec{k}}(\Omega_n)$$

$$\delta\mathcal{A}^{(2)}_{eff} = -\sum_i \Gamma^{(4)}_i(\{\Omega\})\psi_i^4 - \sum_{ij}\Gamma^{(2,2)}_{i,j}(\{\Omega\})\psi_i^2\psi_j^2$$

New equations for AFM instability in KLM read:

$$\frac{\partial}{\partial\mathcal{N}}\left(\frac{\beta\mathcal{N}^2}{4I_M(Q)} + \ln\left(\cosh\left(\frac{\beta\mathcal{N}}{2}\right)\right) + \delta\mathcal{A}[\mathcal{N}]\right) = 0 \qquad (4)$$

where

$$\delta\mathcal{A}[\mathcal{N}] = -\ln\left[1 - J\rho(0)\ln\left(\frac{\epsilon_F}{max[\mathcal{N}, \beta^{-1}]}\right) - \frac{\pi J\rho(0)}{2\cosh(\beta\mathcal{N})}\right] + \sum_{\omega_n\neq 0} ...$$

The equation (15) can be simplified in two limiting cases

$$\mathcal{N} = I_{AFM} Z\tanh\left(\frac{\beta\mathcal{N}}{2}\right)\left[1 - \frac{\delta}{\ln(\frac{T}{T^*})}\frac{\cosh^2(\beta\mathcal{N}/2)}{\cosh^2(\beta\mathcal{N})}\right], \quad \mathcal{N} < \beta^{-1}$$

$$\mathcal{N} = I_{AFM} Z\left[\tanh\left(\frac{\beta\mathcal{N}}{2}\right) - \frac{\alpha}{\beta\mathcal{N}}\frac{1}{1 - J\rho(0)\ln(\epsilon_F\mathcal{N}^{-1})}\right], \quad \mathcal{N} > \beta^{-1}$$

We estimate $T_N/T^0_N \sim 1 - c/\ln(T^0_N/T^*) < 1$. A numerical solution of (15) and modified Doniach [7,8,9] diagram are presented on Fig.2.

M.Kiselev and R.Oppermann, Phys.Rev.Lett 85, 5631 (2000)

$$H = \sum_k \varepsilon(k) c^+_{k,\sigma} c_{k,\sigma} + J \sum_i \vec{S}_i \vec{s}_i + \sum_{ij} I_{ij} \vec{S}_i \vec{S}_j$$

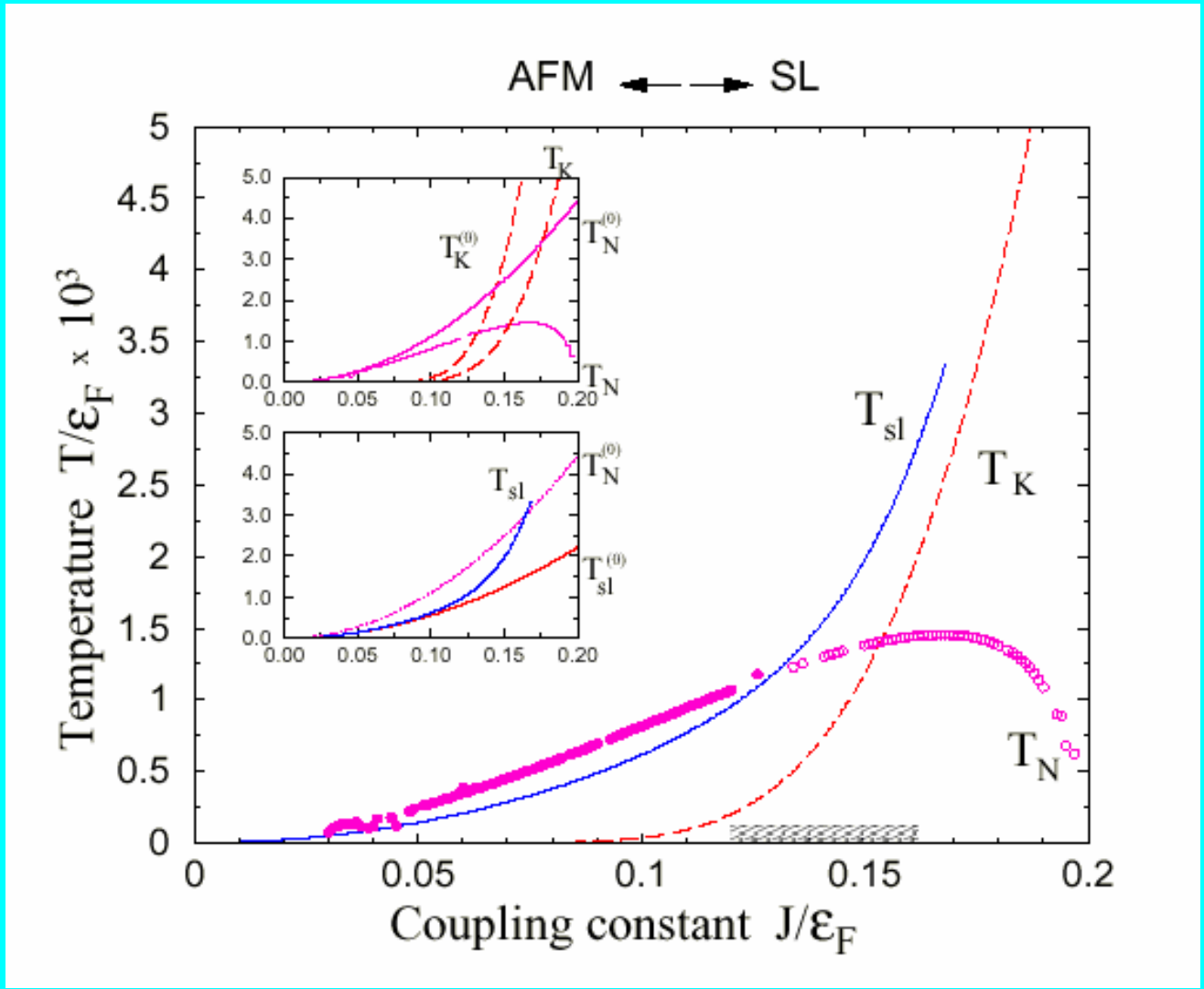

$$H = \sum_k \varepsilon(k) c^+_{k,\sigma} c_{k,\sigma} + J \sum_i \vec{S}_i \vec{s}_i + \sum_{ij} I_{ij} S^z_i S^z_j$$

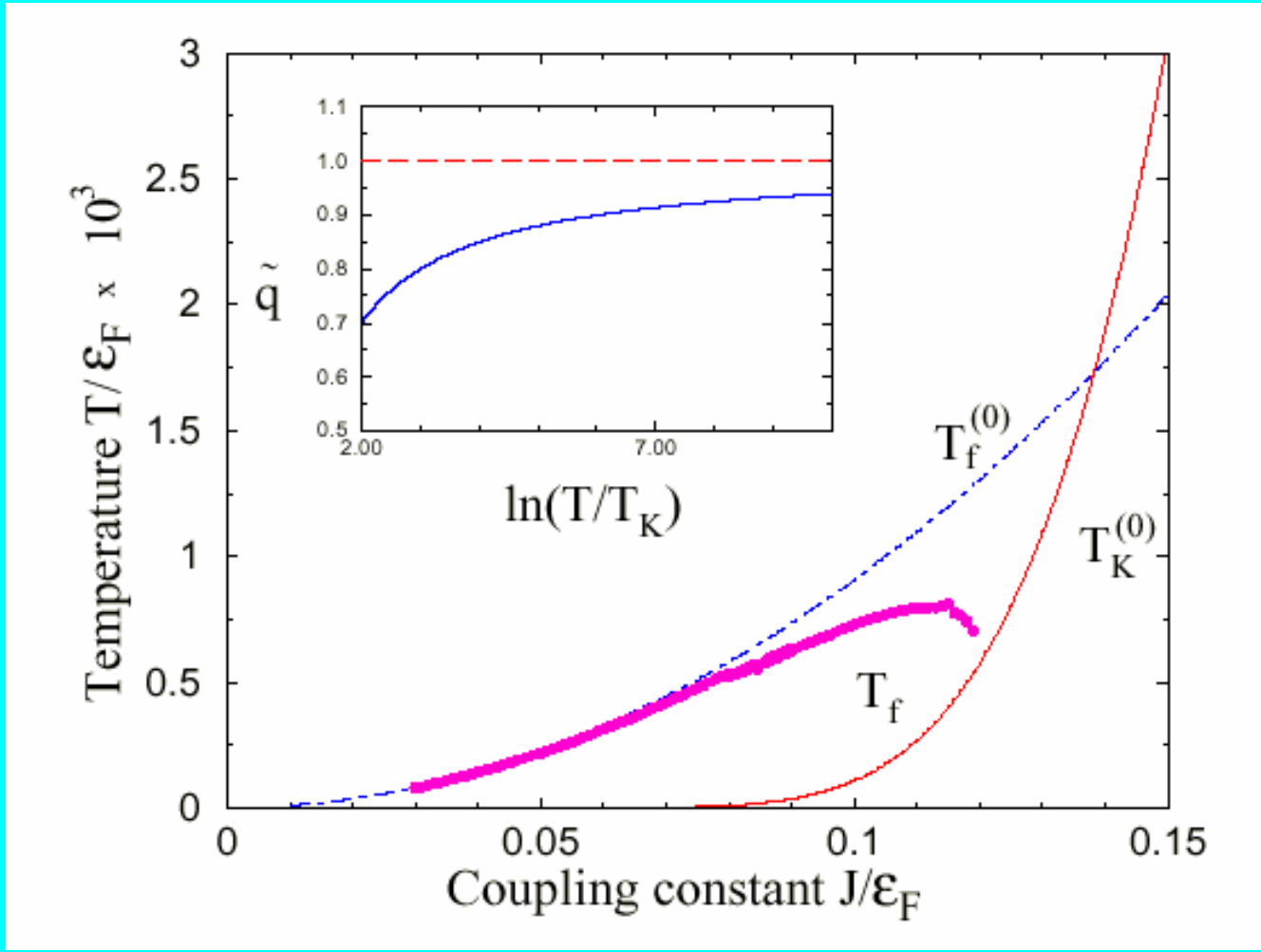

Kondo Wolken

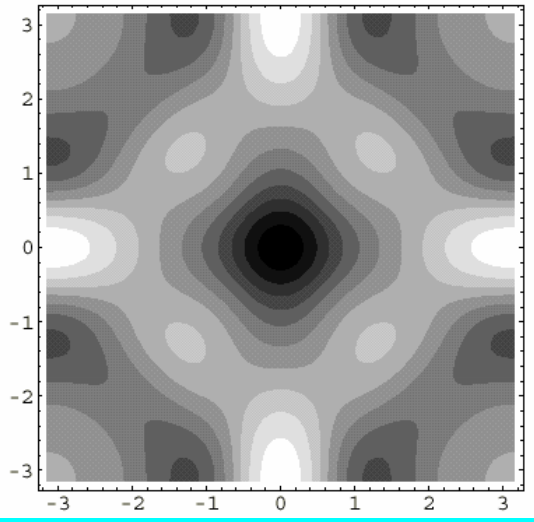

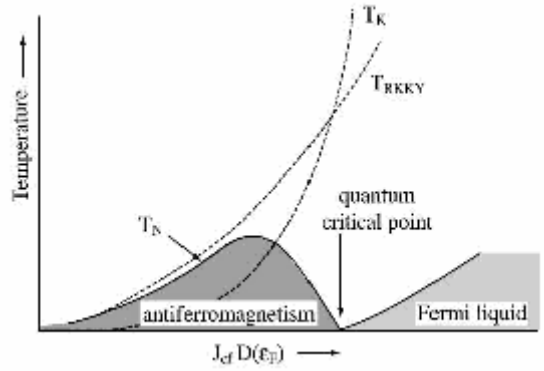

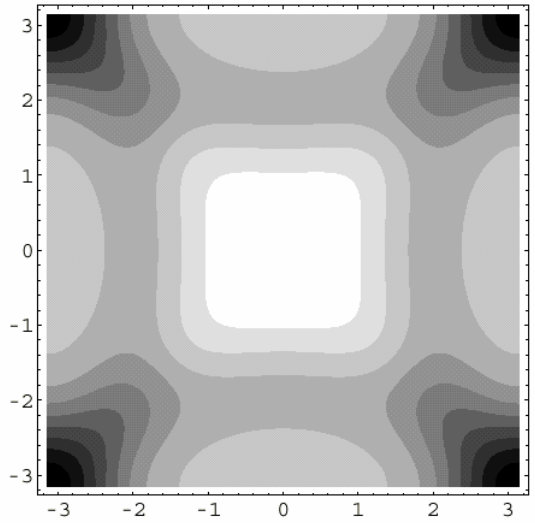

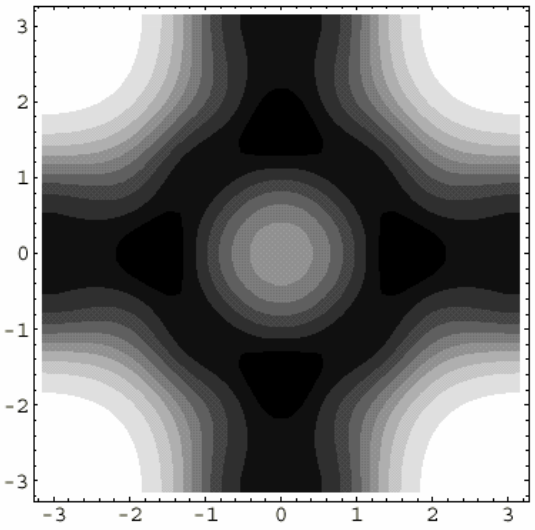

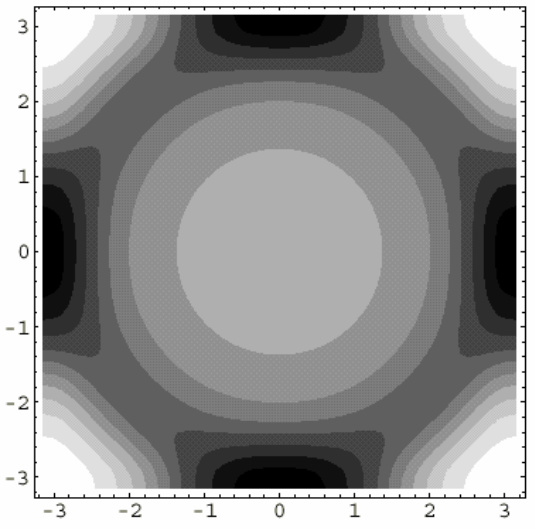

Fragen

- Warum sind die Quasiteilchen so schwer?
- Warum unterscheiden sich die Massen aus Wärmekapazitäts- und dvA-Messungen?
- Warum ist die Fermi-Fläche so groß trotz großer Massen?
- Was ist der Grund für das quanten-kritische Verhalten?

Mögliche Antworten

- Die eigentlichen Quasiteilchen sind “Spinonen”, keine “Elektronen”
- Die quasiteilchen tragen Spin, aber keine Ladung
- Es gibt keine Hybridisierung von “Spinonen” und “Elektronen”
- Quanten kritisches Verhalten resultiert aus der Konkurrenz von Kondo und RKKY WW

3 Single magnetic impurities under the microscope

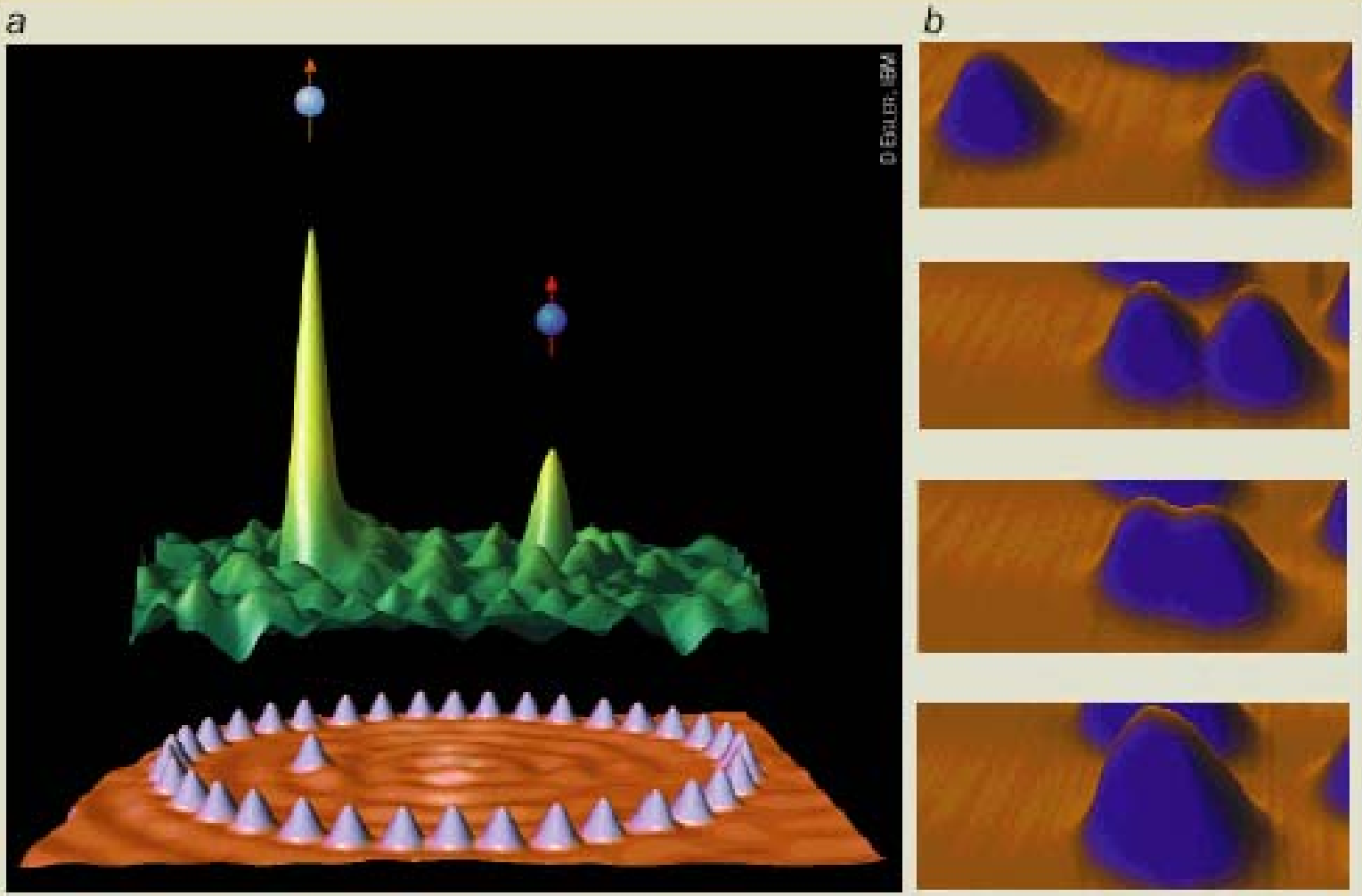

(*a*) By manipulating cobalt atoms on a copper surface, Don Eigler and colleagues at IBM have placed a single cobalt atom at the focal point of an ellipse built from other cobalt atoms (bottom). The density of states (top) measured at this focus reveals the Kondo resonance (left peak). However, elliptical confinement also gives rise to a second smaller Kondo resonance at the other focal point (right) even though there is no cobalt atom there. (*b*) Meanwhile, Mike Crommie and co-workers have measured two Kondo resonances produced by two separate cobalt atoms on a gold surface (top). When two cobalt atoms are moved close together using an STM, the mutual interaction between them causes the Kondo effect to vanish (data not shown).

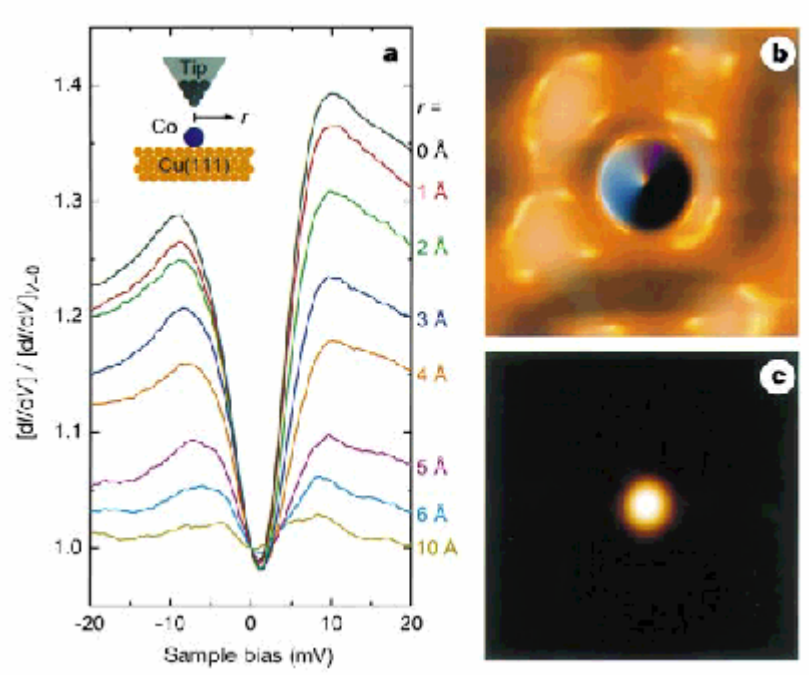

Figure 1 Detection of the Kondo resonance localized around a single Co atom on Cu(111). **a**, Tunnel spectra (normalized d*I*/d*V*) acquired over the Co atom for increasing lateral displacement *r* ($R_T = 100\,M\Omega$ at $V = 10$ mV). Inset, measurement geometry. **b**, 35-Å square topograph ($V = 5$ mV, $I = 1$ nA) of an isolated Co atom (0.8-Å-high central bump) **c**, d*I*/d*V* map of the same area (average of $V = \pm 5$ mV acquisitions, $V_{a.c.} = 1$ mV r.m.s., $I = 1$ nA). Dark to light corresponds to increasing conductance. Examples of the three types of data obtained in this experiment: (1) Topograph images (**b**) were acquired with the scanning tunnelling microscope (STM) operating in constant d.c. current (*I*) mode, in which a closed feedback loop constantly adjusted tip height. (2) Tunnel spectra (**a**) were acquired by adding a small a.c. modulation $V_{a.c.}$ (1 mV r.m.s. at 201 Hz) to the d.c. bias *V*, opening the feedback loop (hence, holding the tip motionless with respect to the surface), and measuring d*I*/d*V* versus *V* through lock-in detection of the a.c. component of the tunnel current. Such spectra were essentially independent of the tunnel junction impedance R_T, determined by *V*/*I* before opening the feedback loop. (3) d*I*/d*V* image maps (**c**) were acquired simultaneously with associated topographs by applying an a.c. modulation (typically 250 μV to 1 mV r.m.s. at 201 or 1007 Hz) at a frequency exceeding the bandwidth of the feedback loop, and recording the lock-in detected d*I*/d*V* (conductance map) along with tip height (topograph) at fixed d.c. bias *V* while the tip was scanned in closed-loop constant-*I* mode. Both kinds of differential conductance measurements constitute a probe of the local density of states under the tip[17,18].

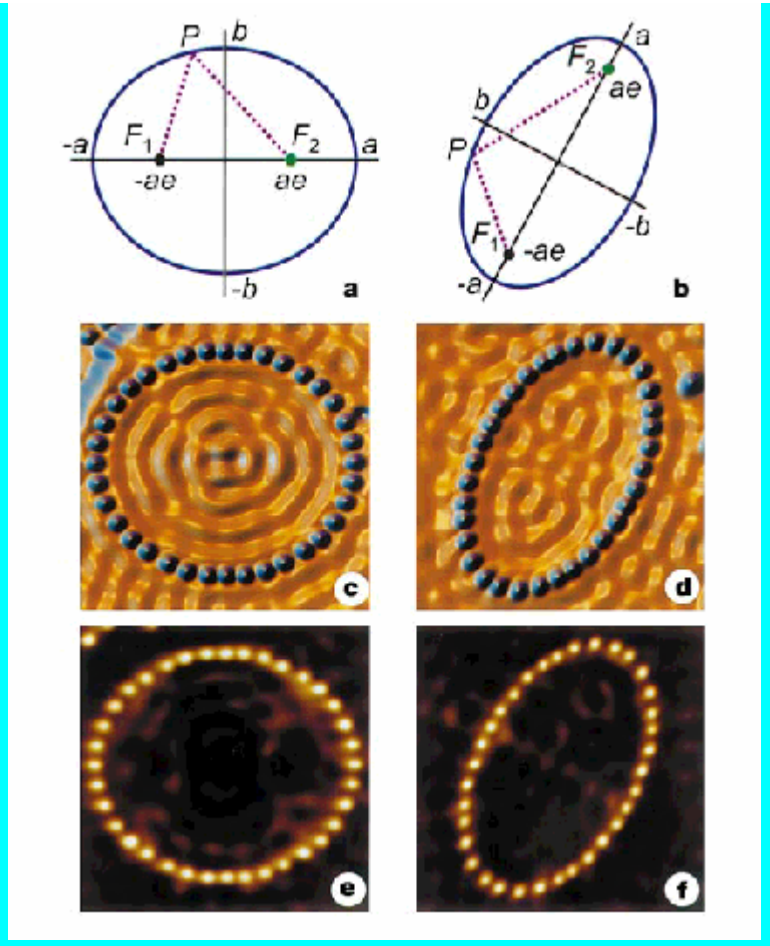

Figure 2 Elliptical electron resonators. **a**, Eccentricity $e = 1/2$; **b**, $e = 0.786$. **c**, **d**, Corresponding topographs of the experimental realizations ($a = 71.3$ Å for both ellipses) employing Co atoms to corral two-dimensional electrons on Cu(111). **e**, **f**, d*I*/d*V* maps acquired simultaneously with the corresponding topographs, tuned to image the Kondo resonance. ($V = 10$ mV, $V_{a.c.} = 250$ μV r.m.s., $I = 1$ nA for **c** and **e**; $V = 8$ mV, $V_{a.c.} = 1$ mV r.m.s., $I = 1$ nA for **d** and **f**). Image dimensions are 150 Å square and 154 Å square for the $e = 1/2$ and $e = 0.786$ ellipses, respectively.

H.Manoharan et al, Nature 403, 512 (2002)

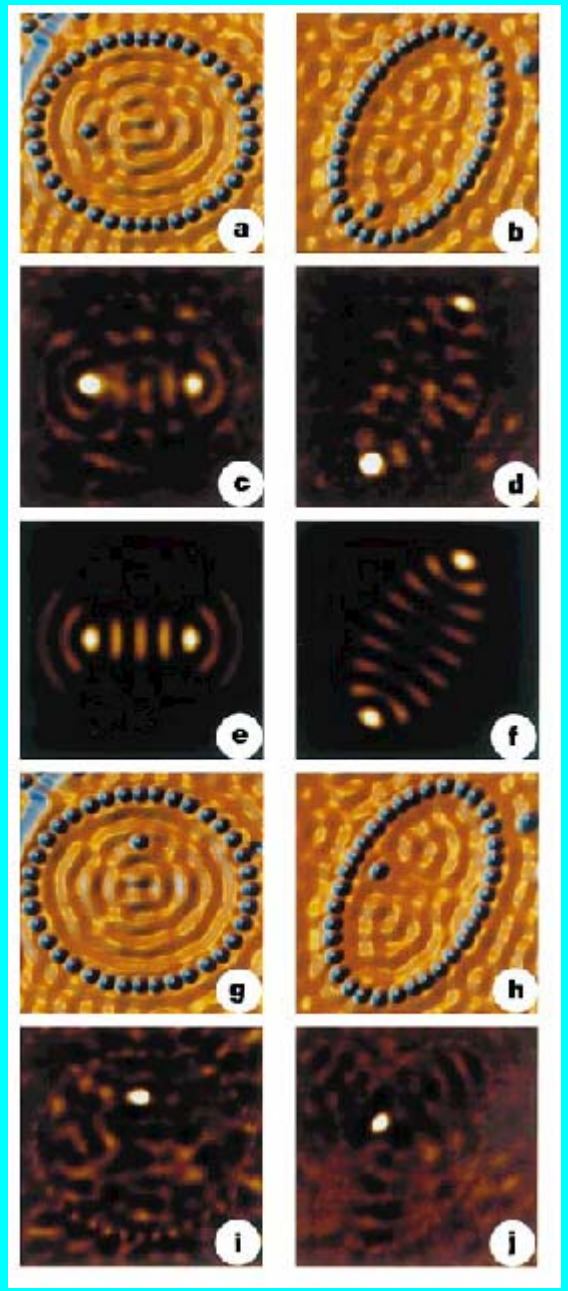

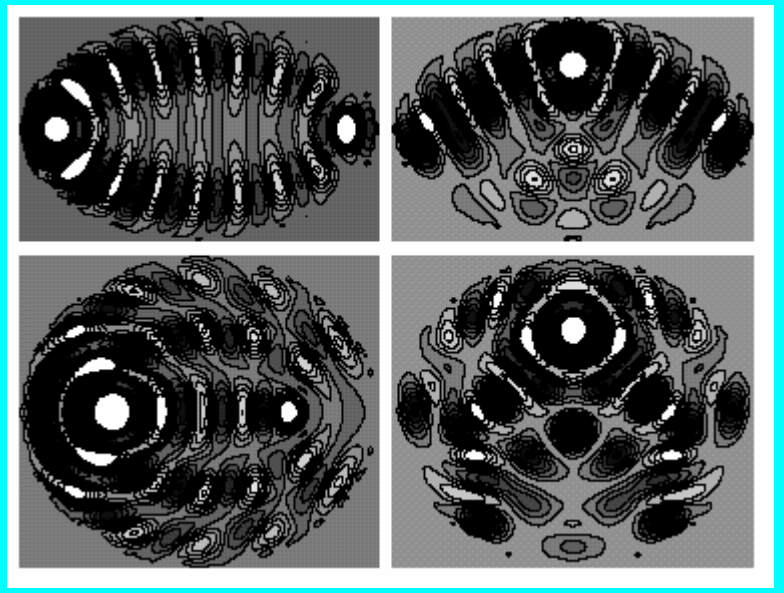

$$\delta\rho(\vec{R},\epsilon_F) \simeq \rho_s \frac{16t^3}{(k_F d)^2}\cos(4k_F a).$$

Figure 3 Visualization of the quantum mirage. **a**, **b**, Topographs showing the $e = 1/2$ (**a**) and $e = 0.786$ (**b**) ellipse each with a Co atom at the left focus. **c**, **d**, Associated d*I*/d*V* difference maps showing the Kondo effect projected to the empty right focus, resulting in a Co atom mirage. **e** and **f**, Calculated eigenmodes at E_F (magnitude of the wavefunction is plotted). When the interior Co atom is moved off focus (**g** and **h**, topographs), the mirage vanishes (**i** and **j**, corresponding d*I*/d*V* difference maps). Imaging conditions and dimensions as in Fig. 2. We have assembled over 20 elliptical resonators of varying size and eccentricity and searched for the formation of a quantum mirage. We find that as *a* is increased monotonically while *e* is fixed, the mirage is switched on and off. In each period of this switching, the classical path length 2*a* changes by a half Fermi wavelength. Because we also observe that two focal atoms, one on each focus, couple quite strongly with one another (as judged by the perturbation of the Kondo resonance) these oscillatory results may have a source akin to the RKKY (indirect exchange) interaction[19].

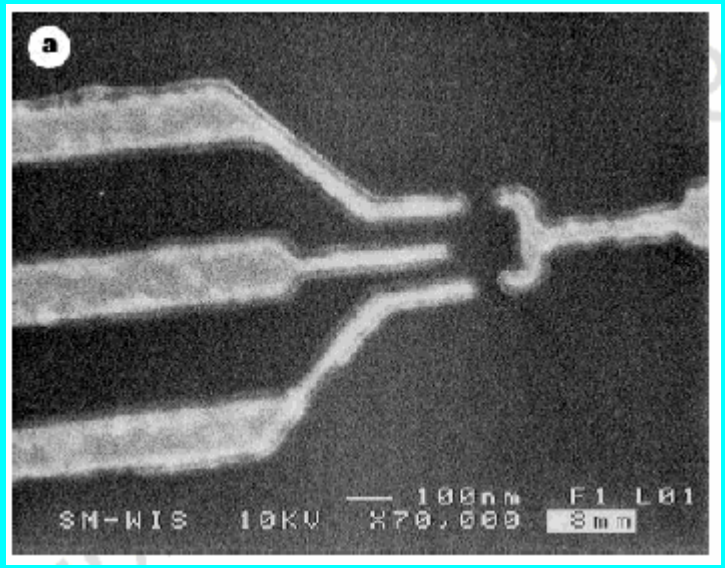

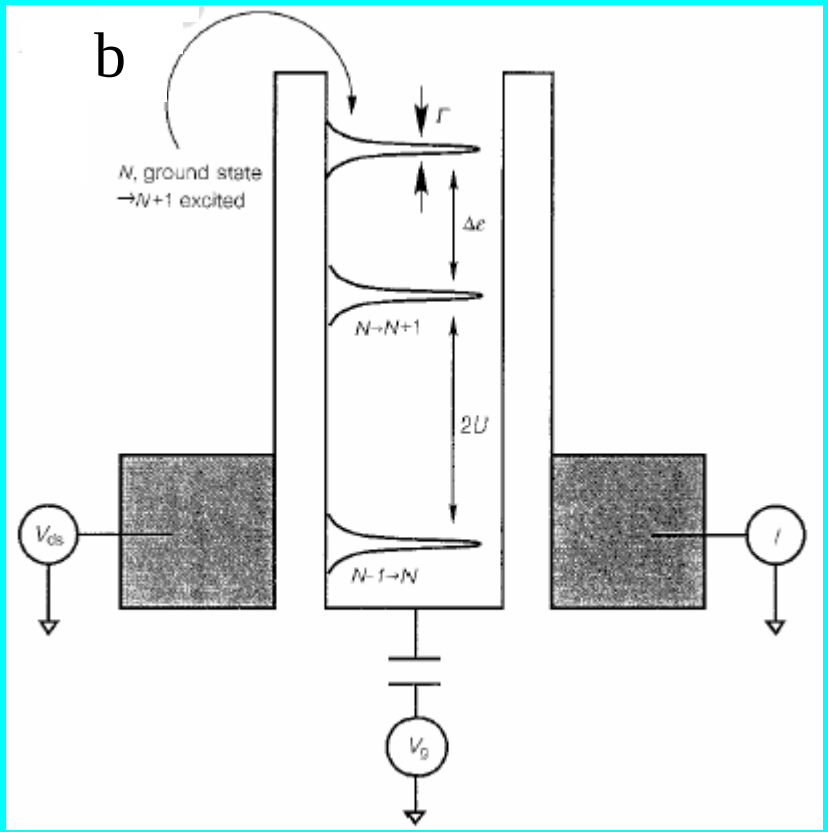

Figure 1 a, Scanning electron microscope image showing top view of sample. Three gate electrodes, the one on the right and the upper and lower ones on the left, control the tunnel barriers between reservoirs of two-dimensional electron gas (at top and bottom) and the droplet of electrons. The middle electrode on the left is used as a gate to change the energy of the droplet relative to the two-dimensional electron gas. Source and drain contacts at the top and bottom are not shown. Although the lithographic dimensions of the confined region are 150 nm square, we estimate lateral depletion reduces the electron droplet to dimensions of 100 nm square. The gate pattern shown was deposited on top of a shallow heterostructure with the following layer sequence grown on top of a thick undoped GaAs buffer: 5 nm $Al_{0.3}Ga_{0.7}As$, $5 \times 10^{12}\,cm^{-1}$ Si δ-doping, 5 nm $Al_{0.3}Ga_{0.7}As$, δ-doping, 5 nm $Al_{0.3}Ga_{0.7}As$, 5 nm GaAs cap (H.S., D.G.-G. and U.M., manuscript in preparation). Immediately before depositing the metal, we etched off the GaAs cap in the areas where the gates would be deposited, to reduce leakage between the gates and the electron gas. **b**, Schematic energy diagram of the artificial atom and its leads. The situation shown corresponds to $V_{ds} < kT/e$, for which the Fermi energies in source and drain are nearly equal, and to a value of V_g near a conductance minimum between a pair of peaks corresponding to the same spatial state. For this case there is an energy cost $\sim U$ to add or remove an electron. To place an extra electron in the lowest excited state costs $\sim U + \Delta\epsilon$.

D.Goldhaber-Gordon et al, Nature 391, 156 (1998)

4 Quantum-dot devices

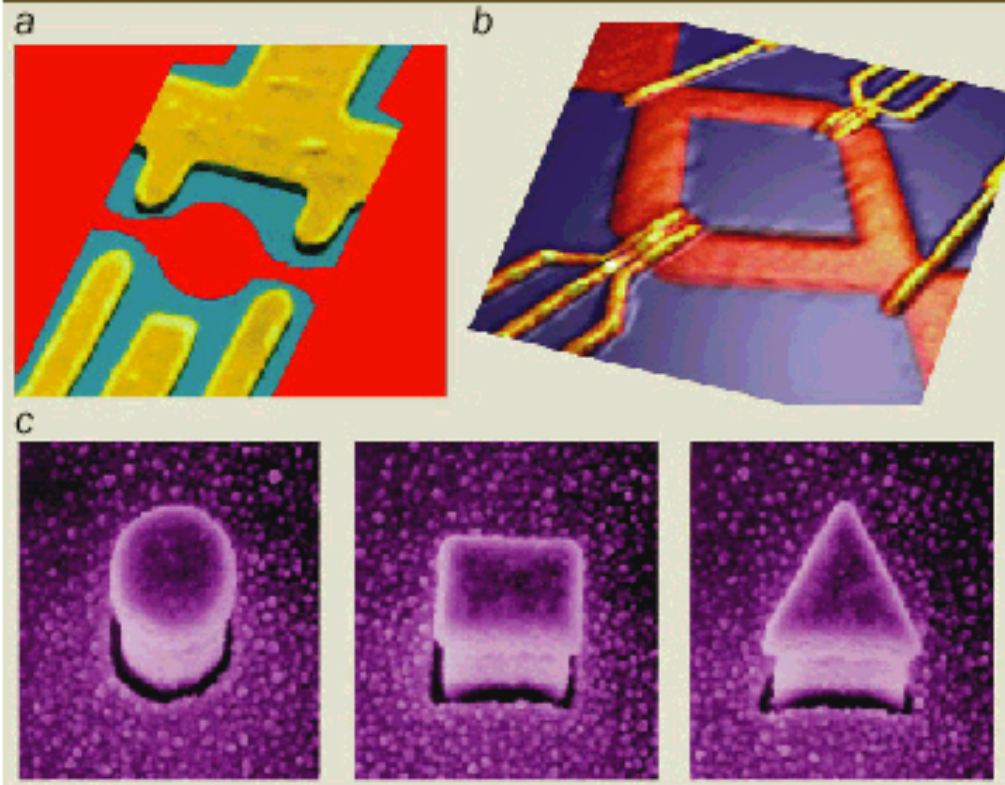

(*a*) A quantum dot can be defined by applying voltages to the surrounding gate electrodes (yellow). The tunnelling between the dot and the external electrodes (top left) is controlled by changing the voltages on the lower-left and lower-right gates. This coupling defines the lifetime broadening, Γ, of the quantum state in the dot. The number of electrons and the energy levels are tuned by the voltage on the lower-central gate. The puddle of electrons (confined red region) is about 0.5 microns in diameter. (*b*) Quantum dots can be placed in both arms of a two-slit interference device. Such a device has been used to investigate whether this scattering destroys the interference pattern. (*c*) Three quantum dots that have been used to compare the Kondo effect for singlet, doublet and triplet spin-states.

5 Universal scaling

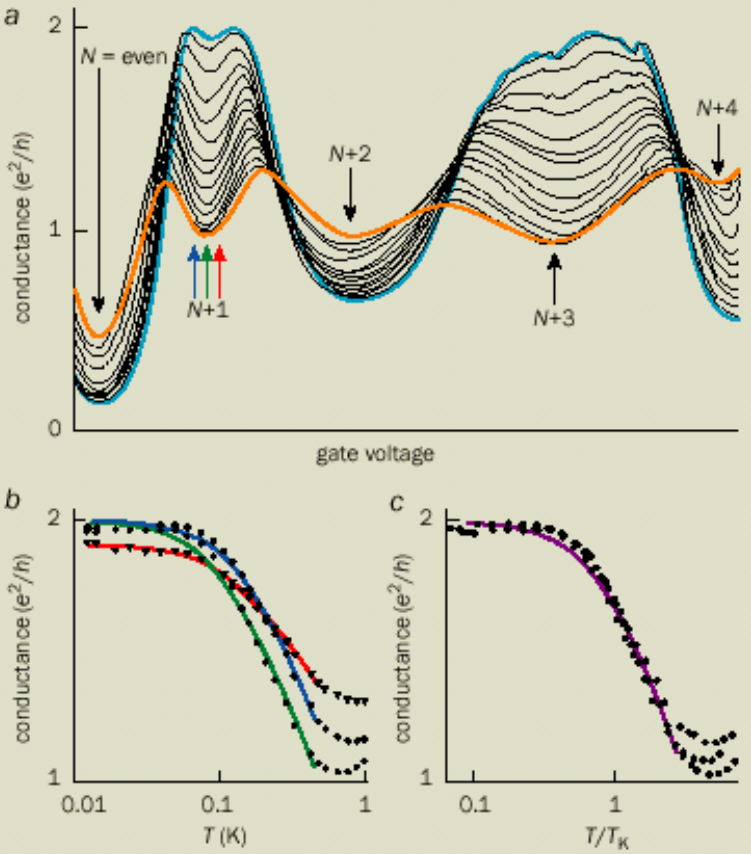

(*a*) The conductance (*y*-axis) as a function of the gate voltage, which changes the number of electrons, *N*, confined in a quantum dot. When an even number of electrons is trapped, the conductance decreases as the temperature is lowered from 1 K (orange) to 25 mK (light blue). This behaviour illustrates that there is no Kondo effect when *N* is even. The opposite temperature dependence is observed for an odd number of electrons, i.e. when there is a Kondo effect. (*b*) The conductance for $N + 1$ electrons at three different fixed gate voltages indicated by the coloured arrows in (*a*). The Kondo temperature, T_K, for the different gate voltages can be calculated by fitting the theory to the data. (*c*) When the same data are replotted as a function of temperature divided by the respective Kondo temperature, the different curves lie on top of each other, illustrating that electronic transport in the Kondo regime is described by a universal function that depends only on T/T_K.

L.Kouwenhoven and L.Glazman, Physics World 35 (2001)

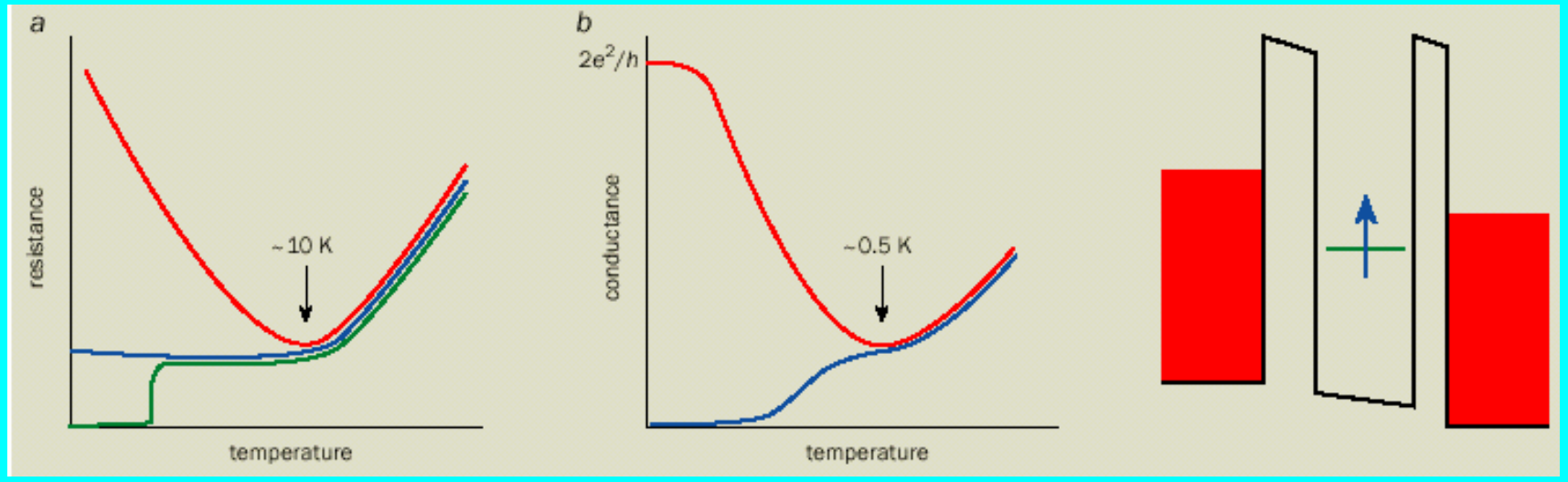

2 Spin flips

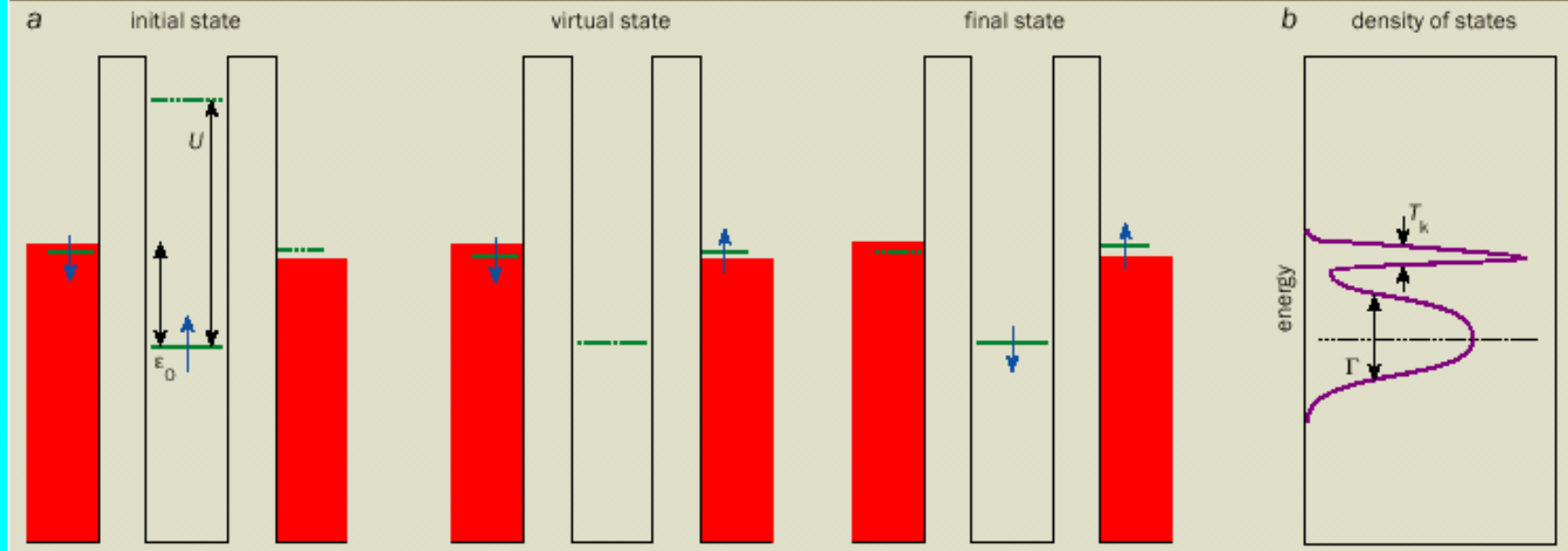

(*a*) The Anderson model of a magnetic impurity assumes that it has just one electron level with energy ε_0 below the Fermi energy of the metal (red). This level is occupied by one spin-up electron (blue). Adding another electron is prohibited by the Coulomb energy, *U*, while it would cost at least $|\varepsilon_0|$ to remove the electron. Being a quantum particle, the spin-up electron may tunnel out of the impurity site to briefly occupy a classically forbidden "virtual state" outside the impurity, and then be replaced by an electron from the metal. This can effectively "flip" the spin of the impurity. (*b*) Many such events combine to produce the Kondo effect, which leads to the appearance of an extra resonance at the Fermi energy. Since transport properties, such as conductance, are determined by electrons with energies close to the Fermi level, the extra resonance can dramatically change the conductance.

VOLUME 74, NUMBER 23 PHYSICAL REVIEW LETTERS 5 JUNE 1995

Resonant Tunneling Through Two Discrete Energy States

N. C. van der Vaart, S. F. Godijn, Y. V. Nazarov, C. J. P. M. Harmans, and J. E. Mooij
Department of Applied Physics, Delft University of Technology, P.O. Box 5046, 2600 GA Delft, The Netherlands

L. W. Molenkamp*
Philips Research Laboratories, 5600 JA Eidenhoven, The Netherlands

C. T. Foxon[†]
Philips Research Laboratories, Redhill, Surrey RH15HA, United Kingdom
(Received 10 January 1995)

We observed new type of Lorentzian-shaped resonances in the current through two coupled quantum dots with tunable barriers. We show that the resonances occur when the energy of two discrete states match. Their widths can be as small as 5 μeV and are only determined by the lifetime of the discrete energy states, independent of the reservoir temperature. The achieved energy resolution makes it possible to observe a small asymmetric deviation from the Lorentzian line shape, which we attribute to inelastic tunnel processes.

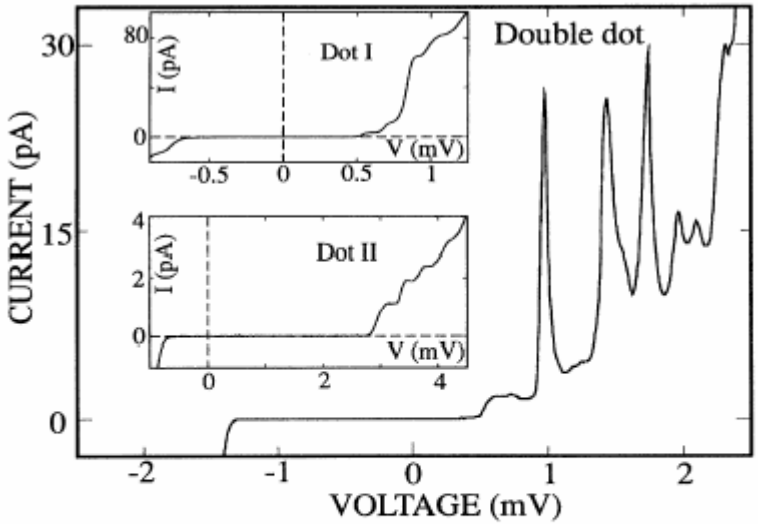

FIG. 2. *I-V* curve of the double dot, showing sharp resonances in the current when two 0D states line up. Upper inset: *I-V* curve of dot I. Lower inset: *I-V* curve of dot II. Both insets show a suppression of the current at low voltages due to the Coulomb blockade and a stepwise increase of the current due to the discrete energy spectrum of the dot.

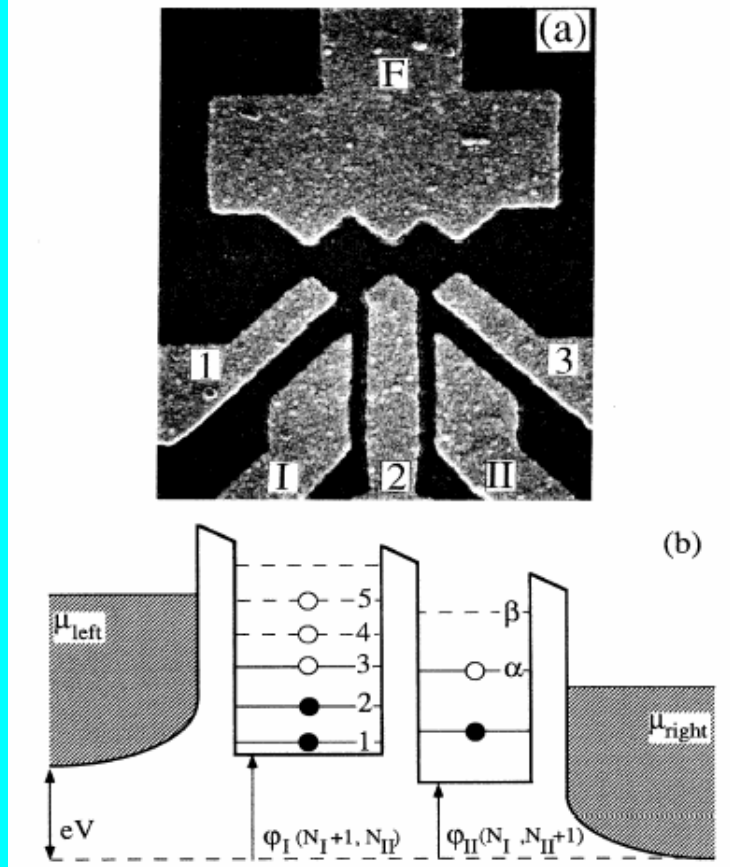

FIG. 1. (a) SEM micrograph of the double dot with lithographic dimensions of 320 × 320 nm^2 (left dot) and 280 × 280 nm^2 (right dot). (b) Schematic potential landscape of the double quantum dot, where μ_{left} and μ_{right} denote the electrochemical potentials of the left and right reservoirs and V the bias voltage across the double dot. The 0D states in dot I are denoted by levels 1 to 5 and in dot II by levels α and β.

Unser Vorschlag für Experimente – Nicht-Gleichgewichts Kondo Effekt in parallelen Quantendots

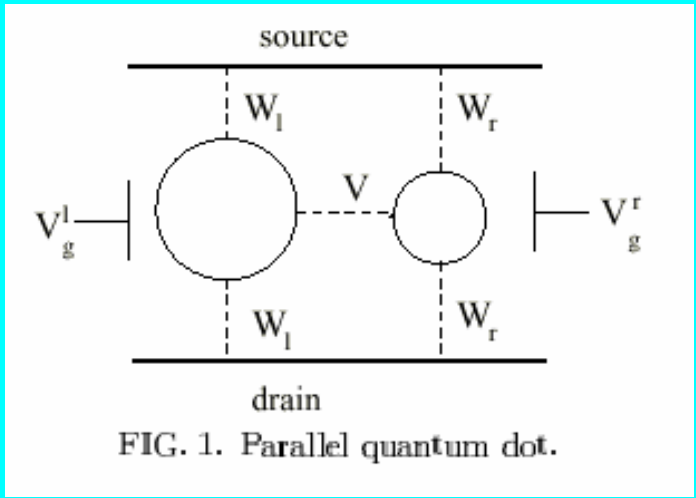

FIG. 1. Parallel quantum dot.

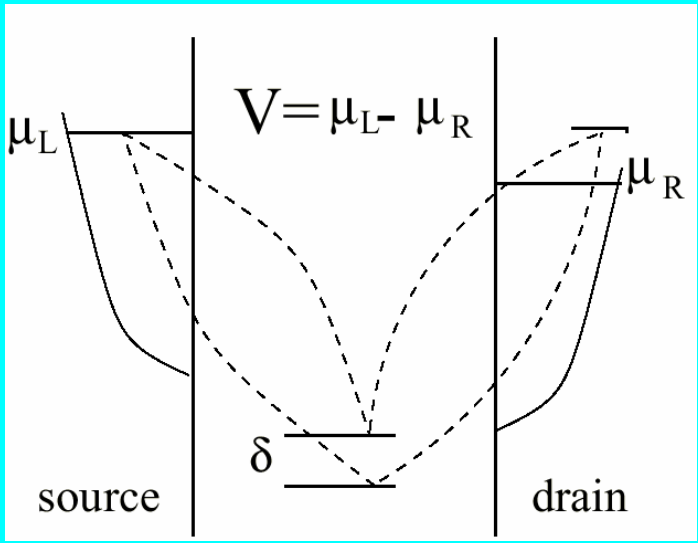

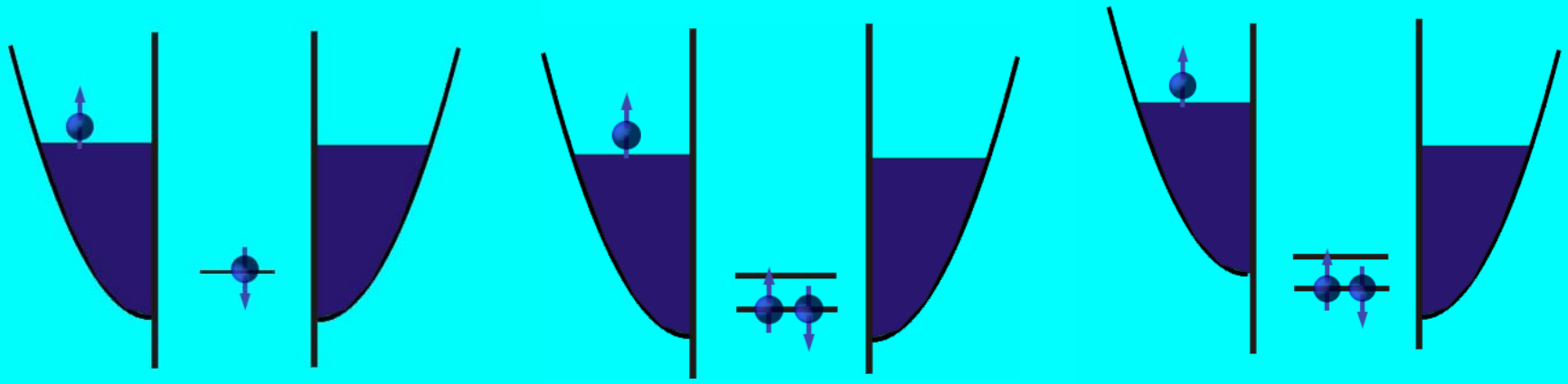

Kein Kondo im Gleichgewicht

Kondo

Nicht-Gleichgewichts Kondo

Zusammenfassung

- Der Kondo-Effekt ist verantwortlich für ungewöhnliche thermodynamische- und Transporteigenschaften von HF Materialen
- Wechselspiel zwischen magnetischen- und Kondo-Korrelationen resultieren in quanten kritischem Regime
- Nano-Technologie bietet noch nie dagewesene Möglichkeiten der Kontrolle von Kondo-Systemen